Global Phosphoproteomic Mapping of Early Mitotic Exit in Human Cells Identifies Novel Substrate Dephosphorylation Motifs[S]

Rachael A. McCloy‡, Benjamin L. Parker§, Samuel Rogers‡, Rima Chaudhuri§, Velimir Gayevskiy‡, Nolan J. Hoffman§, Naveid Ali‡, D. Neil Watkins‡¶‖, Roger J. Daly**, David E. James§, Thierry Lorca‡‡, Anna Castro‡‡, and Andrew Burgess¶‡§§

Entry into mitosis is driven by the coordinated phosphorylation of thousands of proteins. For the cell to complete mitosis and divide into two identical daughter cells it must regulate dephosphorylation of these proteins in a highly ordered, temporal manner. There is currently a lack of a complete understanding of the phosphorylation changes that occur during the initial stages of mitotic exit in human cells. Therefore, we performed a large unbiased, global analysis to map the very first dephosphorylation events that occur as cells exit mitosis. We identified and quantified the modification of >16,000 phosphosites on >3300 unique proteins during early mitotic exit, providing up to eightfold greater resolution than previous studies. The data have been deposited to the ProteomeXchange with identifier PXD001559. Only a small fraction (~10%) of phosphorylation sites were dephosphorylated during early mitotic exit and these occurred on proteins involved in critical early exit events, including organization of the mitotic spindle, the spindle assembly checkpoint, and reformation of the nuclear envelope. Surprisingly this enrichment was observed across all kinase consensus motifs, indicating that it is independent of the upstream phosphorylating kinase. Therefore, dephosphorylation of these sites is likely determined by the specificity of phosphatase/s rather than the activity of kinase/s. Dephosphorylation was significantly affected by the amino acids at and surrounding the phosphorylation site, with several unique evolutionarily conserved amino acids correlating strongly with phosphorylation status. These data provide a potential mechanism for the specificity of phosphatases, and how they co-ordinate the ordered events of mitotic exit. In summary, our results provide a global overview of the phosphorylation changes that occur during the very first stages of mitotic exit, providing novel mechanistic insight into how phosphatase/s specifically regulate this critical transition. ***Molecular & Cellular Proteomics 14: 10.1074/mcp.M114.046938, 2194–2212, 2015.***

Entry into mitosis is driven by the phosphorylation of thousands of proteins on multiple sites, triggering extensive cellular rearrangements including chromosome condensation, microtubule reorganization, and nuclear envelope breakdown (1). Many of these protein phosphorylation events are induced by cyclin dependent kinase 1 (CDK1)[1], which is considered the master regulator of mitosis (2). However, several recent large-scale quantitative phosphoproteomic studies have highlighted the important role of other kinases, such as Polo like kinase 1 (PLK1), Aurora A and B, in driving many of these mitotic events (3–5). For cells to exit mitosis, the phosphorylation sites modified by these kinases must be dephosphory-

From the ‡The Kinghorn Cancer Center, Garvan Institute of Medical Research, Darlinghurst, NSW, 2010, Australia; §The Charles Perkins Center, School of Molecular Bioscience and Sydney Medical School, The University of Sydney, NSW 2006, Australia; ¶St. Vincent's Clinical School, Faculty of Medicine, UNSW, Darlinghurst, NSW, Australia; ‖Department of Thoracic Medicine, St Vincent's Hospital, Darlinghurst, NSW, 2010, Australia; **Department of Biochemistry and Molecular Biology, School of Biomedical Sciences Monash University, Clatyon, VIC, 3800, Australia; ‡‡Equipe Labellisée Ligue Nationale Contre le Cancer, Universités Montpellier 2 et 1, Centre de Recherche de Biochimie Macromoléculaire, CNRS UMR 5237, 1919 Route de Mende, 34293 Montpellier cedex 5, France.

Received December 2, 2014, and in revised form, June 2, 2015
Published, MCP Papers in Press, June 8, 2015, DOI 10.1074/mcp.M114.046938
Author contributions: A.C. and A.B. designed research; R.A.M, B.L.P., S.R., N.J.H., N.A., and A.B. performed research; D.N.W., R.J.D, D.E.J., T.L., and A.C. contributed new reagents or analytic tools; S.R., R.C., V.G., and A.B. analyzed data; A.B. wrote the paper.

[1] The abbreviations used are: CDK, cyclin dependent kinase; PLK1, polo like kinase 1; APC, anaphase promoting complex; ATM, Ataxia telangiectasia mutated; CK1/2, casein kinase 1/2; EME, early mitotic exit; GFP, Green Fluorescent Protein; GSK3, glycogen synthase kinase 3; GO, Gene Ontology; H2B, histone H2B; LC-MS/MS, liquid chromatography-tandem mass spectrometry; MAPK, mitogen-activated protein kinase; OA, okadaic Acid; PKA, protein kinase A; PP1, protein phosphatase 1; PP2A, protein phosphatase 2A; SAC, spindle assembly checkpoint; SILAC, stable isotope labeling by amino acids in cell culture.

Financial Disclosure: This work was supported by the Cancer Institute NSW FRL fellowship ID#10/FRL/3–02 and the Petre Foundation. The funders had no role in study design, data collection and analysis, decision to publish, or preparation of the manuscript.

lated (6). Furthermore, the order of their removal must be different to that of mitotic entry, in order to create the unique mitotic exit events that produce two identical daughter cells (7, 8). The current model of how cells exit mitosis is based on the coordinated degradation and dephosphorylation of proteins. Protein degradation is driven by the anaphase promoting complex (APC) and its associated co-factors CDC20 and CDH1, which co-ordinate the ordered degradation of several key regulatory proteins, including cyclin B and securin (9, 10). Protein degradation removes proteins and hence their phosphorylation status, ensuring that mitotic exit continues in one direction and does not reverse (11, 12). However, currently only ~170 proteins have been found to be targeted for degradation during mitotic exit (13), which although likely to be a significant underestimation, is only well short of the 5000+ proteins phosphorylated during mitosis (14). Therefore, during exit a substantial number of proteins must be dephosphorylated by phosphatases in preparation for the next G1 phase. For many years phosphatases were thought to constantly dephosphorylate substrates. However, recent discoveries have shown they are in fact highly regulated, and must first be inhibited to permit mitotic entry, and then reactivated for mitotic exit (15, 16). For the highly ordered events of mitotic exit to occur correctly, the dephosphorylation of substrates must occur in a rigid, timely, and ordered fashion. Failure to do this results in a catastrophic failure of mitosis (17, 18). This suggests that phosphatases must dictate an order of dephosphorylation for the correct timing of specific mitotic exit events. This concept is supported by recent results in budding yeast where the well characterized mitotic exit phosphatase Cdc14 (19) drives ordered dephosphorylation during mitotic exit (8). Evidence from higher-order mammalian, *Xenopus* and *Drosophila* models indicates that both phosphatase PP2A (20–22) and PP1 (23, 24) are required for mitotic exit, whereas Cdc14 appears to be dispensable (reviewed in (25)). Yet despite many of these recent advancements, we still do not fully understand the mechanisms controlling the global phosphorylation changes that occur during the initial early stages of mitotic exit. Are certain substrates preferentially dephosphorylated, and if so how do phosphatases recognize and specifically dephosphorylate these substrates? To answer these questions we undertook a global, unbiased phosphoproteomic approach to characterize the full repertoire of phosphorylation changes that occur as human cells begin exiting mitosis.

EXPERIMENTAL PROCEDURES

Chemicals, Reagents, and Antibodies—The following chemicals were used: RO3306 (Axon MedChem, Reston, VA), Okadaic Acid sodium salt (A.G. Scientifix, San Diego, CA), Nocodazole (Sigma, St. Louis, MO) Thymidine and 2′-Deoxycytidine hydrate (Santa Cruz Biotechnology, Dallas, TX). Antibodies used in this study are described in supplemental Table S2.

Cell Synchrony—Thymidine block/release synchronizations were performed as previously described (18). For mitotic shake off, HeLa cells were first released from G1/S Thymidine block, and then treated with 100 ng/ml of Nocodazole for 14 h, to capture cells in prometaphase (PM). Floating cells were then removed by shake-off, and treated with 25 μM MG132 for 15 min. Mitotic cells were forced to undergo mitotic exit by addition of 10 μM RO3306.

Western Blot Analysis—Proteins from whole-cell lysates were resolved under reducing conditions on 4–12% Bis-Tris polyacrylamide gels (Life Technologies) using standard methods. Resolved proteins were transferred to 0.45 μm Immobilon-FL PVDF membranes (Millipore) and incubated with the indicated antibodies overnight at 4 °C. Protein bands were detected by the appropriate IRDye (680/800) fluorescently labeled secondary antibody then imaged using an Odyssey CLx (Li-COR). Blots were checked for equal loading by reprobing with anti-β-actin.

SILAC Labeling and Mass Spectrometry—HeLa cells were SILAC-labeled by culturing in DMEM in which the natural "light" Lysine and Arginine were replaced by "heavy" isotope-labeled amino acids 13C615N4-L-Arginine (Arg 10) and 13C615N2-L-Lysine (Lys 8) (Silantes GmBH, Gollierstr, Germany) which was supplemented with 10% dialyzed FBS and 4 mM glutamine. Cells were cultured for approximately six doublings to reach complete labeling of >97% and then synchronized using thymidine and released into Nocodazole (100 ng/ml) for 12 h. Mitotic cells were enriched by shake off, and both light and heavy labeled samples were treated with 25 μM MG132 for 15 min. Heavy labeled samples were then treated with 10 μM RO3306 (RO) for a further 15 min, with both samples then harvested by centrifugation at 4 °C. Three biological replicates were prepared, and in one replicate, the heavy/light labels were switched to provide an internal labeling control. Cells were lysed in urea lysis buffer (2.5 mM sodium pyrophosphate, 1 mM B-glycerol phosphate, 1 mM sodium orthovanadate, 1 mM tris (2-carboxy- ethyl) phosphine (TCEP), 1 mM EDTA, 8 M urea, and 20 mM HEPES), sonicated, and then iodoacetamide was added to 100 mM. Protein concentration was determined by the Bradford assay (Thermo Fisher Scientific, Scoresby, VIC, Australia). Samples were then mixed 1:1 (light/heavy) based on quantification of total protein and digested in-solution with modified TPCK treated trypsin (Promega, Alexandria, Australia). Peptides were desalted on C18 solid-phase extraction columns and separated into 9 fractions by strong-cation exchange (SCX) using the ÄKTApurifier (GE Healthcare, Silverwater, Australia) followed by TiO_2 phosphopeptide enrichment as previously described (26, 27). Peptides were resuspended in 0.5% acetic acid and loaded onto a laser-drawn ~30 cm, 75 μm I.D. fused silica column, packed in house with 3 μm ReproSil Pur-120 C18AQ beads (Dr. Maisch, Germany) using an Easy nLC-II (ThermoFisher Scientific) and eluted with a linear gradient of 0 - 30% acetonitrile containing 0.5% acetic acid. Phosphopeptides were analyzed on an LTQ-Orbitrap Velos Pro (Thermo Fisher Scientific). A precursor MS scan (350 - 1650 m/z) was acquired in the Orbitrap at a resolution of 60,000 followed by data-dependent CID MS/MS in the LTQ of up to 20 most abundant precursor ions. Mass spectra were processed with version 1.2.7.4 of the MaxQuant software package (http://www.maxquant.org) using default settings with the inclusion of match between runs option. Peptides were assigned incorporating modified arginine-10 and lysine-6, with a maximum of two missed cleavages, using the fixed modification carboxyamidomethyl, and variable methionine oxidation and STY phosphorylation. Database searching was performed using the Andromeda search engine integrated into the MaxQuant environment (28) against the complete human proteome containing 88,820 sequence entries (UniProt release-2013_06, ftp://ftp.uniprot.org). Precursor mass tolerance was set at 20 ppm for initial search, fragmentation peptide to 0.6 Da. To ensure high quality protein identifications, MS spectra were also searched against a reverse database of a similar size with the false discovery rate limited to < 1%. Known contaminants identified by

MaxQuant were filtered out of the initial data set. Phosphosite identifications were filtered for greater than 0.75 localization probability and a minimum MaxQuant score of 30 and a maximum posterior error probability of 1% to ensure that only highly confident protein identifications were reported. A fold change cutoff of ≥ 4 ($\log_2$ ratio $\geq +2$ or ≤ -2) was used to identify increased and dephosphorylated phosphopeptides, respectively. A moderated *t* test was used to identify phosphosites that are significantly up or down-regulated using Linear Models for Microarray and RNA-Seq Data (LIMMA) package in R (29). LIMMA allows for global variance shrinkage using an empirical Bayes model. Identified sites were then corrected for multiple hypothesis testing using Benjamini and Hochberg method (controlling for 5% false discovery rate). Phosphopeptides were considered to be stable if they were nonsignificant proteins (adj. P value > 0.05), and had $\log_2$ ratios between -0.25 and $+0.25$ with a standard deviation <0.5. All raw mass spectrometry data files and MaxQuant output files have been deposited to the ProteomeXchange Consortium (http://proteomecentral.proteomexchange.org) via the PRIDE partner repository (30) with the identifier PXD001559. Annotated spectra can be viewed using the free MS-viewer (31) (http://prospector2.ucsf.edu) with the search key gsmtp1s5q7. supplemental Table S1 contains a summary of all the phosphosites identified, along with moderated t-statistics, *p* values and adjusted *p* values for all phosphosites. In addition, each phosphosite is annotated for all potential upstream kinases based on motif, PhosphoSitePlus, and KinomeXplorer prediction methods.

Data Analysis—Data analysis was performed using Microsoft Excel and the bioinformatics platform Perseus (Max Planck Institute of Biochemistry, Munich), and enrichment analysis was performed using Venny (bioinfogp.cnb.csic.es/tools/venny/). Clustering and protein interactions were performed using STRING 9.1 (http://string-db.org/) (32), whereas Gene Ontology (GO) enrichment was performed with Enrichr (http://amp.pharm.mssm.edu/Enrichr/) (33). Motif enrichment analysis of phosphopeptides was performed with MMFPh (34), Icelogo (35) and WebLogo 3 (36). Novel motifs were scanned for potential upstream kinases using the Phospho Motif Finder software incorporated into the HPRD database (http://www.hprd.org/PhosphoMotif_finder), and using KinomeXplorer (http://kinomexplorer.info) (37). Heat maps were created using Matrix2png (38). Geneious version R7.1 was used for sequence alignments of Myc and PRC1 (39). Statistical analysis was performed using GraphPad Prism 6 software using an unpaired nonparametric Kolmogorov-Smirnov *t* test to determine population distribution differences.

Short Peptide Motif Modeling—The short peptides H-Thr-Pro-Pro-OH and H-Thr-Pro-Gly-OH were modeled in ChemBio3D Ultra 14.0.0.117 (CambridgeSoft Dist. By PerkinElmer, Waltham, MA). Each peptide underwent molecular dynamics simulation using MM2 force field calculations (40) in 2.0 fs steps over 10,000 intervals for a temperature of 300 K. The structures were then MM2 energy minimized using a RMS (root-mean square derivative) gradient of 0.01 producing each energy term.

Immunofluorescence Staining—Cells were grown on Histogrip (Life Technologies) coated glass coverslips and fixed using ice-cold 100% methanol (Lamin A/C) or with 3.7% formaldehyde diluted in PBS with 0.5% Triton X-100 for 10 min (Aurora B, Kif23). All cells were washed and then blocked (3% BSA, 0.1% Tween 20 in PBS) for 30 min. Cells were incubated with primary antibodies for 2 h at room temperature in blocking solution. DNA was stained with DAPI. For Lamin A/C staining, a Leica DM6000 SP8 confocal with a 63× lens was used. All other images were captured using Leica DM5500 microscope coupled with a Coolsnap HQ2 camera, using a Leica 100× or 40× APO 1.4 lens, powered by Leica LAS AF v3 software. In all cases 0.3 μm Z-sections were taken, deconvolved, and displayed as 2D maximum projections using Image J (v.1.49), and Adobe Photoshop CC 2014 software.

Live Cell Imaging—Hela cells co-expressing pH2B_mCherry_IRES_neo3 (Addgene plasmid # 21044) and pmEGFP_a_tubulin_IRES_puro2b (Addgene plasmid # 21042), gifts from Daniel Gerlich (41), were filmed with using a Leica TCS SP8 MP confocal microscope coupled with Leica HyD nondescanned detectors and a HC PL APO 63x/1.20 W motCORR CS2 lens powered by LAS AF v3 software. Images, both Tubulin-GFP and H2B-CherryFP fluorescence, were taken every 2.5 min. The resulting images were processed, analyzed and false colored using Image J (v1.49) and Adobe Photoshop CC 2014 software.

RESULTS

Establishment of a Synchronized, Phosphatase Dependent Mitotic Exit Model—In order to study the phosphorylation changes that occur during initial early stages of *m*itotic *e*xit (EME), we created highly enriched populations of mitotic cells using a two-step synchronization process, which were then treated with the proteasome inhibitor MG132, to minimize the loss of phosphorylation from protein degradation. Normal mitotic exit is triggered by the loss of CDK1 activity (42), therefore, we took advantage of the specific CDK1 inhibitor RO3306 (43) to induce a highly synchronized mitotic exit (Fig. 1*A*). A similar method has been used by several other groups to analyze various aspects of mitotic exit (44–46). This model allowed us to perform highly reproducible biochemical analysis of EME, with cells beginning to rapidly exit mitosis within 5 min of CDK1 inhibition. At 10 min, clear invagination of the plasma membrane could be observed at the center of the cell, along with elongation of the mitotic spindle (Fig. 1*B*, supplemental Video S1). Chromatin remained clearly condensed until 30–45 min, at which point the mitotic spindle had largely regressed, and a clear cytokinesis furrow had formed. Furthermore, dephosphorylation of phospho-Histone H3 (Ser10) reached a plateau between 45–60 min, which corresponded with the decondensation of chromatin by time-lapse microscopy (Fig. 1*C*). Inhibition of the proteasome by MG132 was confirmed by the presence of stable cyclin B1 and securin throughout the time course (Fig. 1*C*), with stable securin explaining the failure to separate chromosomes (47). Therefore, our EME model followed the general pattern of a normal mitotic exit, with cells reorganizing the mitotic spindle and forming the midspindle/cytokinesis furrow prior to decondensation of the DNA.

This exit was driven by the activity of phosphatases, as it could be inhibited by cotreatment with the phosphatase inhibitor Okadaic Acid (Fig. 1*D*). Given these results, the time point of 15 min was chosen for subsequent mass spectrometry (MS) analysis, as cells showed clear evidence of EME events including changes in the mitotic spindle, formation of a cytokinesis furrow, yet still contained significant levels of pH3 and condensed chromosomes.

Phosphoproteomic Analysis of the EME—To accurately quantify the global phosphorylation changes during EME, we metabolically labeled cells using stable isotope labeling by amino acids in cell culture (SILAC). SILAC labeled cells were

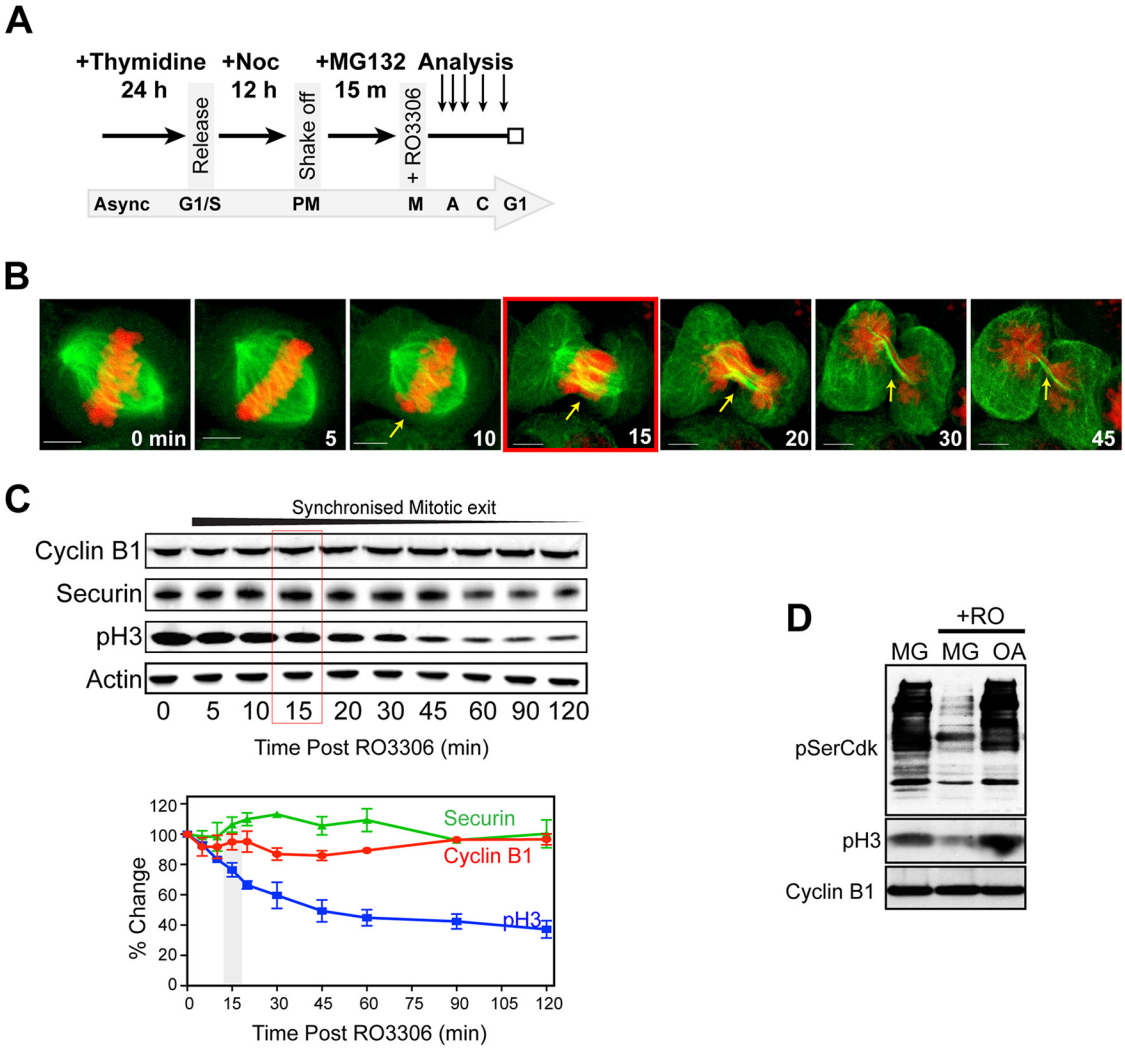

FIG. 1. **A synchronized, phosphatase dependent mitotic exit model.** *A*, Schematic diagram of method for producing highly synchronized HeLa cells undergoing mitotic exit. *B*, Similar to *A*, HeLa cells expressing H2B-mCherry (red) and Tubulin-gfp (green) were synchronized with thymidine, and as cells entered mitosis, protein degradation was blocked with MG132 (MG) for 15 min. Metaphase cells were then treated (0 min) with RO3306 (RO) and followed by time-lapse microscopy. 0.3 μm z-sections were acquired at each time point and displayed as 2D maximum projections. Yellow arrows indicate invagination of plasma membrane at sight of cleavage furrow. Red box indicates approximation of anaphase. Scale bars = 5 μm. *C*, HeLa cells were treated as per A, then harvested at the indicated times post-release, lysed, and analyzed by Western blot with the indicated antibodies. Densitometry of 3 independent experiments was performed, normalized to actin and expressed as a percentage of 0 min time point. *D*, Cells were synchronized as per *A*, and treated with or without okadaic acid (OA, 500 nM). Fifteen minutes later samples were treated with RO for 120 min, then harvested, lysed, and analyzed by Western blot with the indicated antibodies. All error bars are S.E.

treated either with (MG+RO) or without (MG) the CDK1 inhibitor RO3306 for 15min and then harvested. Following SILAC cell harvesting, protein contents of each isotopically labeled heavy and light cell population were equally mixed 1:1, and precipitated proteins were trypsinized. The resulting peptides were desalted using C18 columns, fractionated by strong-cation exchange, and then phosphopeptides were enriched using titanium dioxide (TiO_2) chromatography. Enriched phosphopeptides were analyzed by tandem MS (LC-MS/MS) (Fig. 2*A*).

A combined total of 40,982 phosphosites were identified across three biological replicates. The majority of phosphopeptides contained two or less phosphorylated residues (Fig. 2*B*). Therefore, only high quality phosphopeptides with a PEP score <0.01 and phosphorylation localization score >0.75 were included. The data set contained 141 contaminants and reverse database hits (FDR of 0.84%), which reduced the data set to 16,716 unique phosphorylation sites (supplemental Table S1). Approximately 84% of phosphopeptides were identified on Serine (S) residues, with ~15% on Threonine (T) and <1% on Tyrosine (Y) residues (Fig. 2*B*). Of the 16,716 phosphorylation sites identified, 12,711 are currently annotated in the PhosphoSitePlus database (PSP, phosphosite.org) (48). Therefore, this study has identified an additional

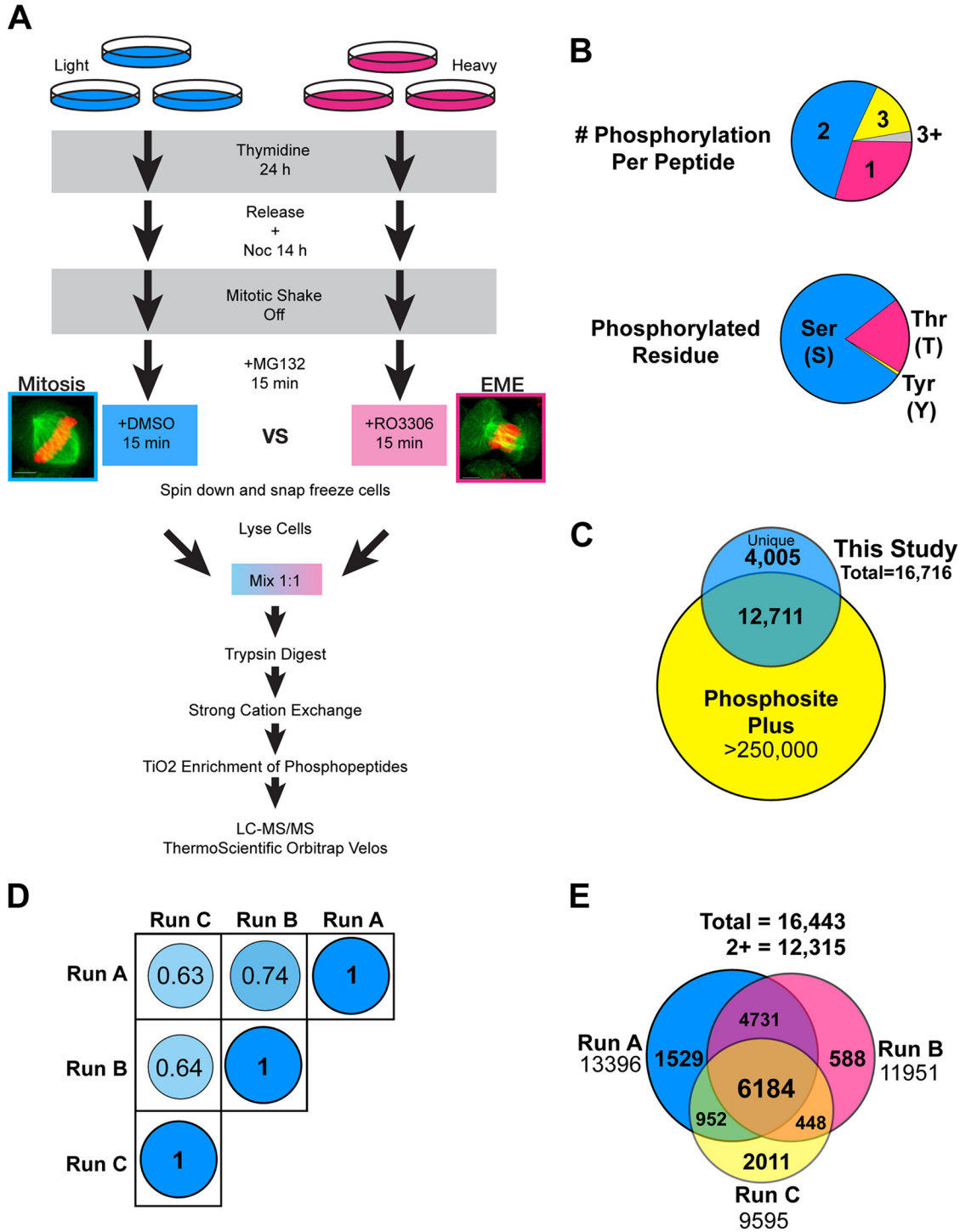

FIG. 2. **Phosphoproteomic analysis of the metaphase to anaphase transition.** *A*, Schematic diagram detailing SILAC metabolic labeling of mitotic and EME samples, followed by peptide digestion, fractionation, phosphopeptide enrichment, and finally quantification by LC-MS/MS. *B*, Proportion of phosphopeptides phosphorylated on Tyrosine (Y), Threonine (T), and Serine (S) residues, and the number of phosphorylation sites identified on each phosphopeptide. *C*, Comparison of the full data set with the PhosphoSitePlus database. *D*, Pearson correlation analysis between independent biological triplicates. *E*, Venn diagram showing the overlap between each of the three independent replicates (runs). Only phosphopeptides that were found in at least two of the runs with <2 standard deviations from the mean, were included for further analysis.

4005 novel mitotic phosphorylation sites that have not previously been annotated in the PSP database (Fig. 2*C* and supplemental Table S1).

Although there have been several other large-scale mitotic phosphoproteomic screens (3, 49), to date only one other study has specifically analyzed the phosphorylation changes

during mitotic exit (50). However, the analysis performed by Malik *et al.* was limited to proteins bound to the mitotic spindle (50). In contrast, in the current study we analyzed whole cell phosphorylation, resulting in a ~six- to eightfold increase in protein and phosphorylation information respectively (supplemental Fig. S1*A*). Consequently, this study provides both a significant increase in resolution and depth, and a unique focus on the global phosphorylation changes that occur specifically during EME.

Reproducibility of Experimental System—To ensure accuracy of the experimental system three independent biological replicates, including a SILAC label switch (Run B), were performed on SILAC labeled cells. Normalized $\log_2$ transformed heavy to light (H/L) ratios were present for more than 98% of the 16,716 phosphorylation sites identified, and each experiment showed a similar spread of ratios (supplemental Fig. S1*B*). An investigation of the variation between the 3 biological replicates found the correlation between samples was 67% on average, and the missing value counts were acceptable (Fig. 1*D* and supplemental Fig. S1*C*). The small difference seen between experiments is likely because of contamination with small, variable amounts of interphase cells during the mitotic shake off enrichment procedure. In summary, the final data set contained quantitative phosphorylation data in at least two experiments for 12,315 sites on 2355 unique proteins (Fig. 2*E*).

Prediction of Upstream Kinase—We began the analysis of this large data set by separating all of the phosphopeptides based on the predicted upstream kinase responsible for each phosphorylation event. To do this we first utilized all of the known kinase-substrate relationships annotated in the PSP database, however; only 654 of the 12,315 sites identified contained a known upstream kinase. Therefore, to include as much of the data as possible we segregated all sites into either Proline (S/T-P) or non-Proline (Non-P) directed kinase families. These were then further separated into the major mammalian kinases (CDK1, GSK3, MAPK, PLK1, Aurora, CKII, PKA, and ATM) using the minimal reported consensus phosphorylation motif for each kinase (supplemental Fig. S2). We were able to assign ~53% of all the identified phosphopeptides as potential substrates for one of these kinases (Fig. 3*A* and supplemental Table S1). To identify potential remaining kinases in the unassigned pools, motif analysis was performed using MMFPh software on all of the phosphopeptides from our data set that did not fit the minimal consensus motif of CDK1, MAPK, GSK3, PLK1, CK2, Aurora, or PKA. MMFPh identifies over-represented amino acid/position pairs in order to identify all statistically significant, sufficiently frequent motifs present in a large phosphoproteomic data set (34). Proline directed sites contained an additional 16 (SP) and 12 (TP) motifs (supplemental Fig. S3*A*); however, all of these additional motifs were likely phosphorylated by the one of the major Proline direct kinases GSK3, MAPK or CDK1 (HPRD) (51). In contrast, only four of the 15 Serine, and one of the five Threonine based Non-P motifs were associated with a potential kinase (supplemental Fig. S3*B*). Searching the PhosphoSitePlus database helped identify several validated kinase and substrates relationships for the majority of these novel motifs. Kinases from all families were random distributed across the motifs suggesting that hierarchical clustering of motifs does not provide any additional enrichment (supplemental Fig. S3*B*). Interestingly, several of the motifs (*e.g.* S-x-x-K/R and S/T-x-P) were associated with CDK1, suggesting that these sites are residual CDK1 sites. In support, a recent paper identified these atypical motifs can be phosphorylated by CDK1 (52). Finally, to further validate our predictions we utilized the KinomeXplorer platform to predict potential cellular kinase-substrate relationships based on motif and cellular context (37). Using this method we were able to identify 127 potential upstream kinases that belong to 50 different kinase families for ~60% of the phosphosites in our data set. The majority of sites were assigned to the MAPK, CDK, PKA, and CK1/2 family of kinases, yet surprisingly only 32 Aurora sites and no PLK1 sites were identified despite their well-known roles in mitosis (Fig. 3*B* and supplemental Table S1). Comparison between the different methods showed varying degrees of agreement, with KinomeXplorer enriching for similar motifs to the minimal reported kinase motifs (supplemental Fig. S2*A* and S2*B*). In addition, both methods were able to identify validated kinase-substrate relationships annotated in the PSP database (Fig. 3*C*). Taken together, these results suggests that both basic motif and more advanced prediction models are able to successfully enrich for validated substrates of the upstream kinase, albeit with varying levels of success.

Impact of Upstream Kinase on Dephosphorylation—The above data demonstrate that multiple upstream kinases are responsible for phosphorylating >12,000 sites during mitosis. To determine if phosphorylation status of specific phosphosites correlated with any specific upstream kinase, we first limited the data set to phosphosites that showed consistency (<2 standard deviations from the mean) between replicates. The final data of 11,954 phosphorylation sites on 2823 proteins was then analyzed using the kinase predictions (both motif and KinomeXplorer based) made above. A statistically significant shift in the cumulative distribution toward dephosphorylation was observed for S/T-P compared with Non-P directed sites, indicating that S/T-P sites were preferentially dephosphorylated during EME (Fig. 4*A*). Separation of phosphosites into each upstream kinase motif also revealed several significant differences. Surprisingly, potential substrates of Aurora kinase (from both prediction methods) along with all unassigned peptides showed a significant shift toward dephosphorylation compared with total Non-P directed sites during EME. Potential PKA and PKC sites were also shifted toward dephosphorylation, but only the KinomeXplorer based prediction method was statistically significant. Finally, TTK (Mps1) sites (KinomeXplorer) were also significantly shifted

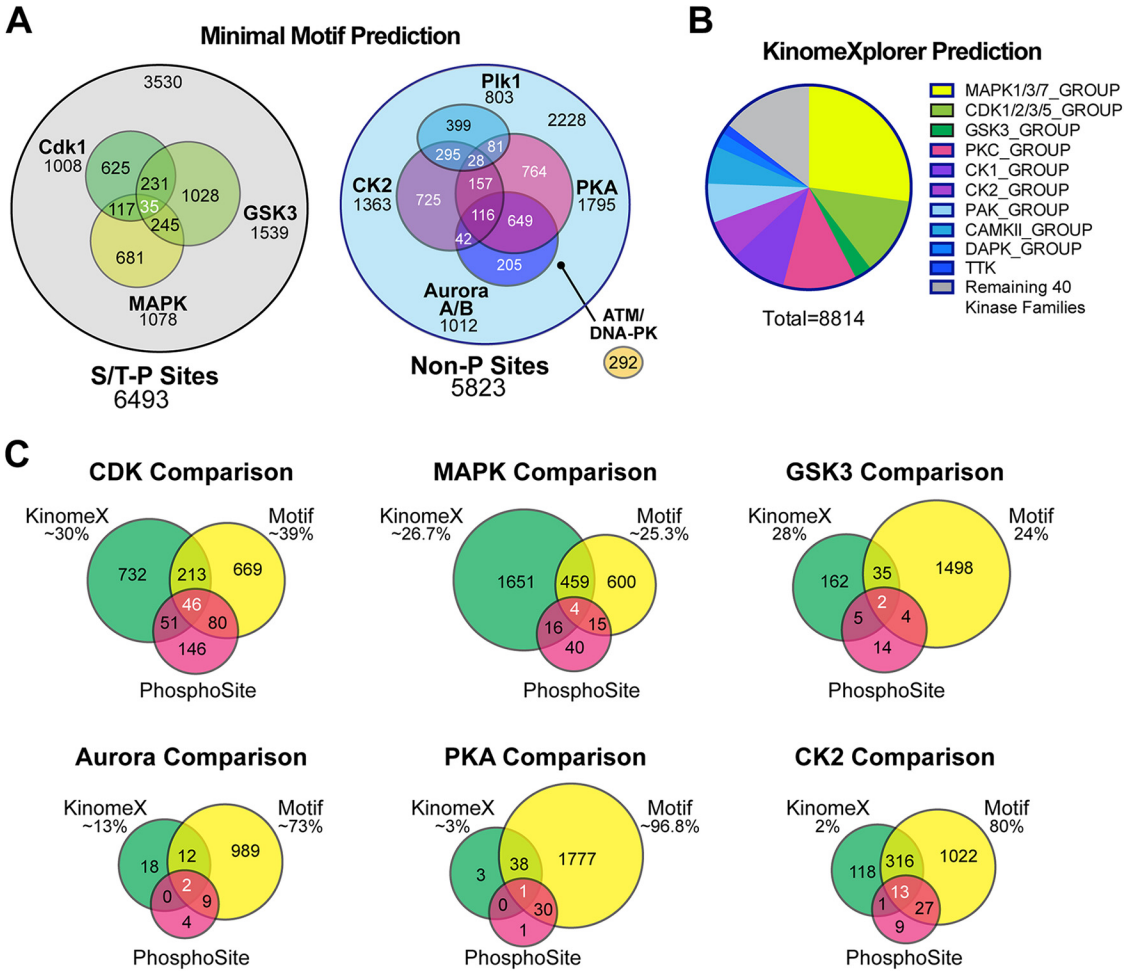

FIG. 3. **Analysis of all unassigned Non-Proline directed phosphopeptides.** *A*, Phosphopeptides were assigned to a potential upstream kinase based on the known minimal consensus motifs for each kinase listed. These were then subdivided into either proline-directed (S/T-P) or nonproline directed (Non-P) sites. *B*, Summary of results from KinomeXplorer based prediction of upstream kinase *C*, Comparison of minimal motif and KinomeXplorer predictions for major S/T-P and Non-P directed kinase with annotated kinase-substrate relationships from the PhosphoSitePlus (PSP) database.

toward dephosphorylation. In contrast, phosphorylation sites targeted by both PLK1 and CK1 and CK2 were significantly shifted to the right and therefore more stable compared with global Non-P sites (Fig. 4*A*). PLK1 has a well-established role during mitotic exit, and its activity is required for correct cytokinesis furrow formation (53). Therefore, it is possible that high PLK1 activity may counterbalance phosphatase activity resulting in stabilization of phosphorylation status. In support, phosphorylation of PLK1 on T210, a marker of PLK1 activity, was stable by both MS analysis (mean $\log_2$ ratio: −0.653) and Western blot analysis, indicating that the majority of PLK1 was still active during EME (Fig. 4*B*). Notably, potential CK2 phosphosites showed an even greater distribution shift than PLK1, suggesting that CK2 activity is also high during mitotic exit.

For Proline directed motifs both GSK3 and all unassigned sites showed no significant difference to total S/T-P sites; however, both CDK1 and to a lesser extent MAPK sites were significantly more stable during EME (Fig. 4*A*). Phosphorylation of the inhibitory Y15 residue on CDK1 was weakly detected at 15 min and noticeably increased after 45 min by Western blot, which correlated with the slight increase in $\log_2$ score observed by MS (Fig. 4*B*). Therefore, it is possible that the stability of the majority of CDK1 phosphosites is because of continued activity of CDK1 kinase. However, the dose of RO3306 used in our system is sufficient to completely block mitotic entry and specifically inhibit >90% of CDK1 kinase activity (18, 43). Given that the addition of RO3306 rapidly triggered mitotic exit, it is likely that most of CDK1 is inhibited in our samples. In summary, these data indicate that during EME the majority of phosphosites from all potential upstream kinases remain stable. The activity of Non-P directed kinases do appear to play a more significant role in dictating the phosphorylation status during EME. In particular, continued PLK1 and potentially CK2 activity, likely explains the stability of these sites. In contrast, the phosphorylation status of S/T-P

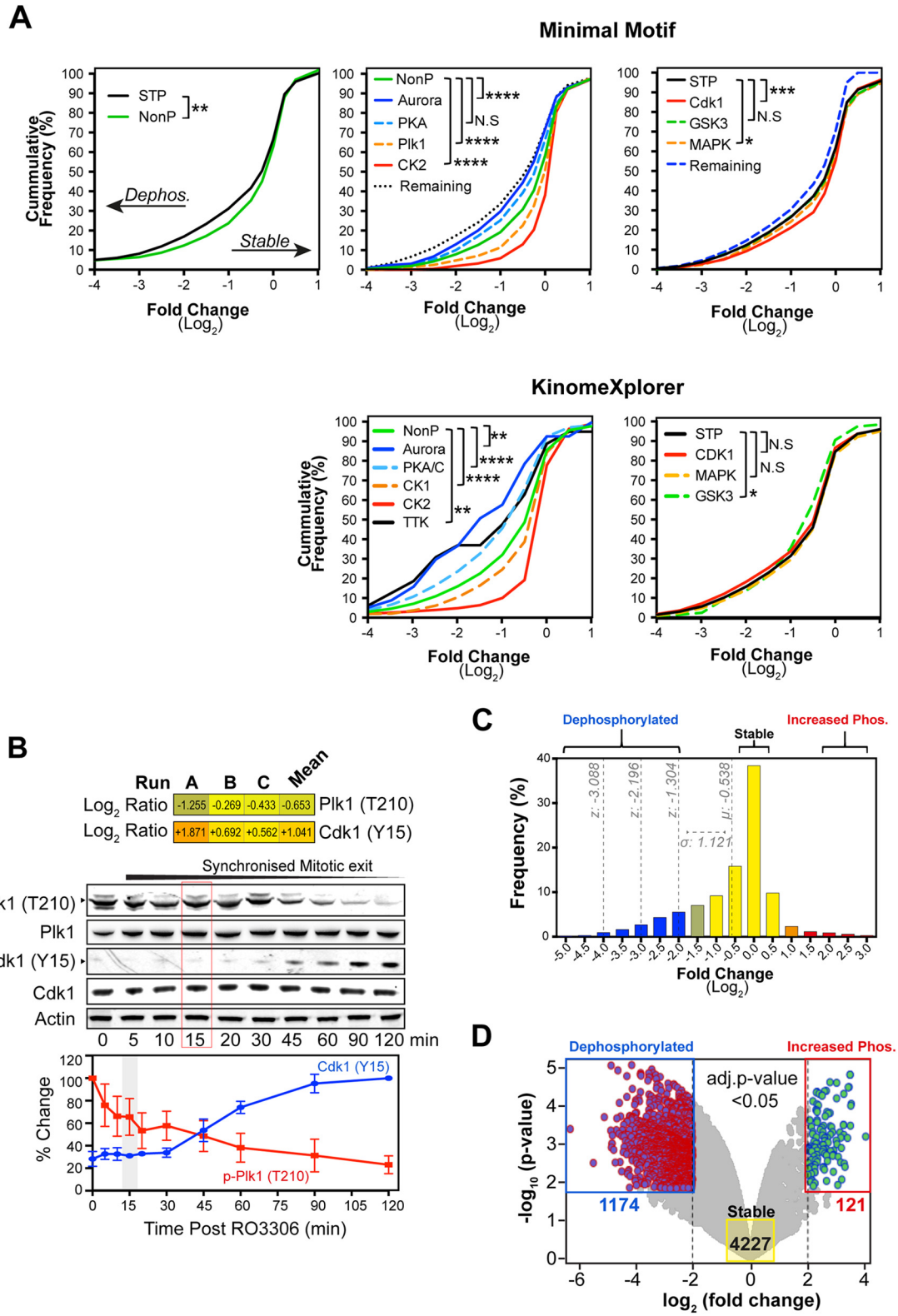

FIG. 4. **Only a small percentage of phosphosites are dephosphorylated during EME.** *A*, Cumulative frequency distribution graphs for all phosphopeptides separated according to potential upstream phosphorylating kinase. Significant differences in the population distributions are shown. *p* values * = <0.01, ** = <0.001, *** = <0.0001, **** = <0.00001, NS = not significant. *B*, Log_2 ratios from each replicate and their mean are shown for phosphorylation at PLK1 (T210), and CDK1 (Y15). HeLa cells were treated as per Fig. 1*A*, then harvested at the indicated times postrelease, lysed, and analyzed by Western blot with the indicated antibodies. Densitometry of three independent experiments was

directed sites, especially CDK1 sites, appears to be independent of the upstream kinase indicating that additional factors determine the specificity of dephosphorylation during EME.

Dephosphorylation of Specific Substrates Drives EME—The above results suggest that changes in the activity of the upstream kinase, especially S/T-P directed sites, are not sufficient to fully account for the specificity of dephosphorylation during EME. To explore this further, we identified phosphorylation sites that were significantly altered during EME. A fold change cut off of a ≥four-fold decrease ($\log_2$ ratio ≤ −2) was used to classify dephosphorylated phosphopeptides, whereas phosphopeptides were considered to be stable if they had consistent (s.d <0.5) $\log_2$ ratios between −0.25 and +0.25, and increased phosphorylation was limited to phosphopeptides with a $\log_2$ ratio ≤ +2 (Fig. 4*C*). A one sample moderated *t* test (with Benjamini/Hochberg correction) was then performed to identify high confidence (adj. *p* value <0.05) differentially expressed phosphosites. Approximately 9.5% of all phosphosites (>4 fold and 5% FDR) were found to be significantly dephosphorylated during EME (Fig. 4*D* and supplemental Table S1).

Analysis of upstream kinases for the significantly dephosphorylated sites, found that there was approximately equal distribution of potential kinases for both motif and KinomeXplorer based prediction methods, with the exception of CK1/2, which was notably reduced in both (Fig. 5*A*). This data again supports the idea that dephosphorylation during EME is not solely dictated by the activity of the upstream kinase. Therefore, we next determined if these dephosphorylated sites were enriched for any specific functional groups of proteins independent of the upstream kinase. This was done by segregating dephosphorylated phosphosites into S/T-P and Non-P directed sites and then comparing any commonly dephosphorylated proteins. This produced a list of 156 proteins that are commonly dephosphorylated independent of the upstream kinase (Fig. 5*B*). STRING analysis (32) of these proteins resulted in strong clustering into several interconnected groups known to regulate EME events (Fig. 5*B*). These included proteins critical for the regulation of the spindle assembly checkpoint (SAC), nuclear pore organization, and microtubule dynamics (Fig. 5*B* and 5*C*). We performed a similar enrichment on common proteins that remained stable during EME and found that they were strongly enriched for proteins involved in regulating RNA processing, nucleic acid metabolism, gene expression, and DNA replication (Fig. 5*C* and supplemental Fig. S4). Furthermore, there was a clear separation between dephosphorylated and stable proteins according to specific cellular compartments, with proteins localized at the central spindle and nuclear pore basket all significantly enriched in the dephosphorylated pool. In comparison, stable phosphorylation sites were highly enriched for ribonucleoproteins, nuclear specks and the nucleolus (Fig. 5*D*). Taken together, these results suggest proteins that regulate and are localized near the mitotic spindle, kinetochores and nuclear envelope are preferentially dephosphorylated during EME.

Dephosphorylation of EME Proteins Correlates with Specific Mitotic Exit Events—The above results suggest that specific proteins are preferentially dephosphorylated during EME; however, these data were based on a single phosphorylation site. The majority of proteins are phosphorylated on multiple sites, and there were 50 proteins that appeared in both dephosphorylated and stable groups (supplemental Figs. S4 and S5*A*). Therefore, we examined all of the phosphorylation sites across a selection of proteins that have known critical roles in regulating the SAC, nuclear envelope and central-spindle formation. Although the majority of proteins contained at least one site that was dephosphorylated, there was a large amount of variability in the phosphorylation states of neighboring sites within each individual protein. Therefore, we ordered proteins by their median $\log_2$ phosphorylation ratio to identify and rank proteins that were strongly dephosphorylated (Fig. 6*A*). Using this method, the top ranked dephosphorylated protein was the nuclear pore component NUP107. Interestingly, NUP107 is one of the first proteins recruited to chromatin and is required for the initiation of nuclear pore complex reassembly during mitotic exit (54). Therefore, we analyzed the other major components of nuclear pore reassembly (POM121C, NUP53, NUP93, and NUP188) and found that the amount of dephosphorylation at 15 min tightly corresponds with the specific order of recruitment of these proteins to the reforming nuclear pore during mitotic exit (Fig. 6*B*). In support, partial reformation of the nuclear envelope was observed in our model during EME (Fig. 6*C*).

We further validated this ordering of proteins, based on the level of dephosphorylation, using band shift as a marker of phosphorylation by Western blot. Both TPX2 and CDC27 were rapidly dephosphorylated within 15 min, with significant loss of the slower migrating phosphorylated band, whereas INCENP showed a gradual stepwise decrease in band shift, matching the heterogeneous dephosphorylation observed at 15 min by MS. BUBR1 remained in its slowly migrating phosphorylated state, with partial dephosphorylation only observed after ~90 min (supplemental Fig. S5*B*). The stability of

performed, normalized to actin and expressed as a percentage of 0 min time point for PLK1 (T210) and against the 120 min time point for CDK1 (Y15). All error bars are S.E. C, Phosphopeptides with $\log_2$ fold change scores of <-2 were considered to be significantly dephosphorylated (blue). Those with $\log_2$ scores between −0.25 and +0.25 were classified as stable (yellow), and those >+2 were classified as having increased phosphorylation (red). Mean (μ), standard deviation (σ) and z-score cutoffs are shown. *D*, Volcano plot showing phosphosites that are significantly up or down-regulated, based on results from a moderated *t* test with correction for multiple hypothesis testing (Benjamini & Hochberg method), controlling for 5% FDR.

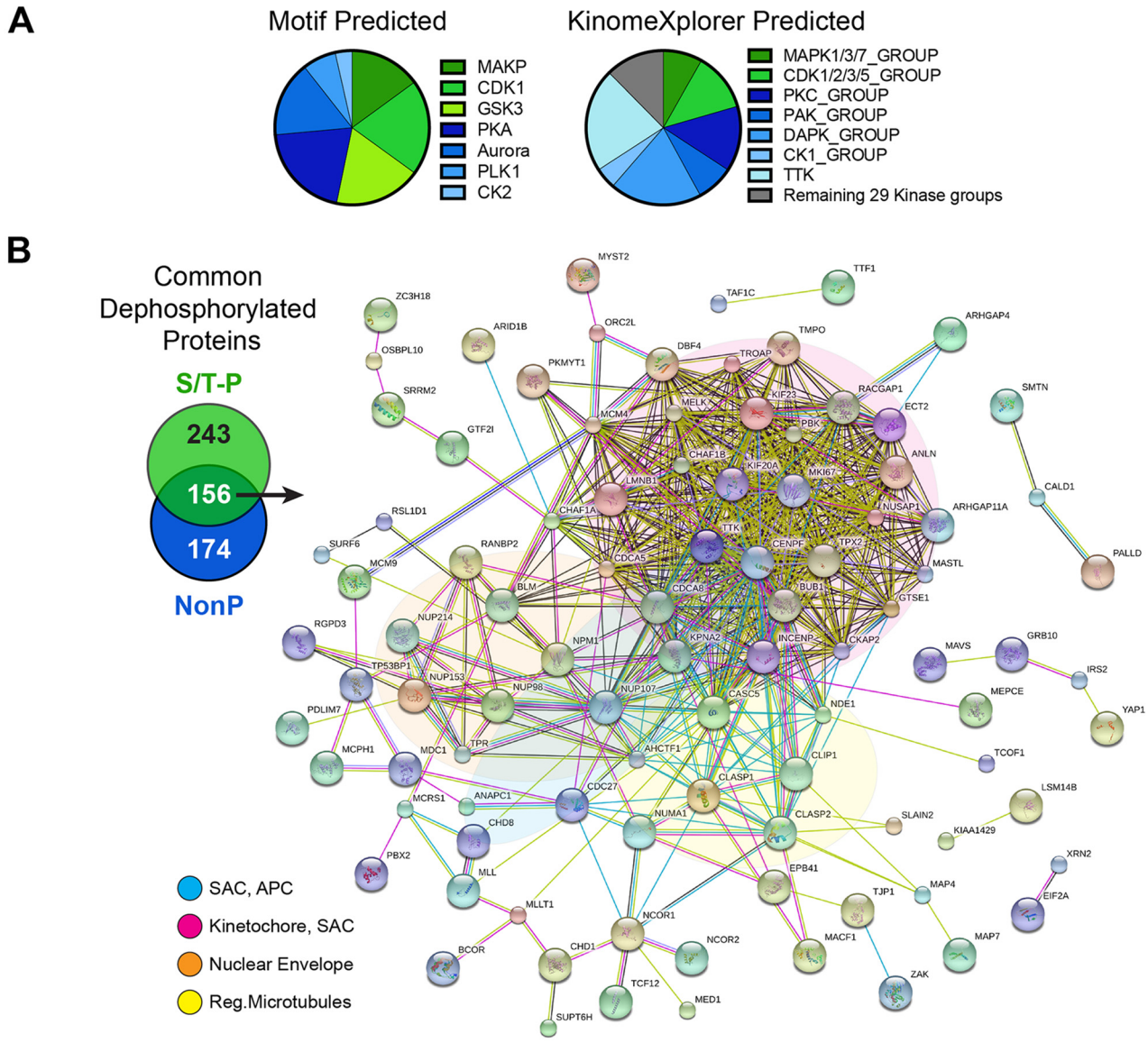
A
Motif Predicted
MAKP
CDK1
GSK3
PKA
Aurora
PLK1
CK2
KinomeXplorer Predicted
MAPK1/3/7_GROUP
CDK1/2/3/5_GROUP
PKC_GROUP
PAK_GROUP
DAPK_GROUP
CK1_GROUP
TTK
Remaining 29 Kinase groups
B
Common Dephosphorylated Proteins
S/T-P
243
156
174
NonP
SAC, APC
Kinetochore, SAC
Nuclear Envelope
Reg.Microtubules
C
GO- Biological Function
*Neg.Reg. M/A
*SAC
*Nuc.Pore Ass.
*Chromosome seg.
*Reg. microtubules
*Chrom.Remodeling
Organelle fission
RNA transport
*mRNA splicing
*Gene expression
Stable
Dephosphorylated
1.0E-00
1.0E-02
1.0E-04
1.0E-06
1.0E-08
1.0E-10
1.0E-12
Adj. P-Value (FDR)
D
GO- Cellular Component
Kinetochore
Spindle
Nuclear pore
*Cell division plane
*Nuclear speck
Centrosome
*Nuclear body
*Heterochromatin
Adherens junction
Cytosol
Stable
Dephosphorylated
1.0E-00
1.0E-02
1.0E-04
1.0E-06
1.0E-08
1.0E-10
1.0E-12
Adj. P-Value (FDR)

BUBR1 phosphorylation was surprising as phosphorylated BUBR1 has been reported to inhibit the APC, thereby blocking anaphase onset (55). However, phosphorylation of BUBR1 at S670 was recently shown to be required for targeting the phosphatase PP2A-B56 to kinetochores (56), where PP2A is required for opposing MPS1 (TTK) activity and silencing of the SAC (57). In support, we found that BUBR1 remained localized at the kinetochore during EME (supplemental Fig. S5*C*). Interestingly, we found that MPS1 was significantly dephosphorylated on S281 (adj. *p* value 0.01, Fig. 6*A*), which would allow the binding of CDC27 and subsequent APC mediated degradation of MPS1 during later stages of mitotic exit (58). Notably, our MS results show that CDC20 is significantly dephosphorylated (adj. *p* value 0.019) on S51 (Fig. 6*A* and supplemental Table S1). This was confirmed using a phosphospecific antibody against the S51 site in CDC20, which showed rapid dephosphorylation within 5 min of triggering mitotic exit with RO3306 (Fig. 6*D*). This dephosphorylation of CDC20 likely ensures prompt and efficient activation of APC and subsequent degradation of MPS1 (58). Subsequent loss of MPS1 activity (through dephosphorylation and degradation) then shifts the balance toward dephosphorylation of downstream SAC proteins at the kinetochore. In support, significant dephosphorylation of several sites on BUB1 and the PP2A-B56 substrate CASC5 (knl1) (57), were observed in our MS results (Fig. 6*A* and supplemental Table S1). Furthermore, this rapid loss of MPS1 activity likely explains the global shift toward dephosphorylation of potential MPS1 (TTK) substrates identified by KinomeXplorer (Fig. 4*A*). Thus, efficient silencing of the SAC during EME appears to be dependent on the preferential dephosphorylation of MPS1 and CDC20. Finally, to examine the formation of the central-spindle, immunofluorescence analysis was performed on KIF23 (Mklp1) and Aurora B. Both proteins underwent rapid relocalization to the central-spindle indicating that, as implicated by our MS results, KIF23 is rapidly dephosphorylated during EME (supplemental Fig. S5*D*). Taken together, these results provide strong evidence that dephosphorylation plays a critical role in determining the order of events during mitotic exit by precisely dephosphorylating specific sites on a subset of substrates involved in regulating EME. However, strong dephosphorylation of a specific site within a protein does not guarantee that the remaining sites within that protein will also be dephosphorylated.

Specific Motifs Correlate with Intra-Protein Phosphosite Status—One possible explanation for the heterogeneity in intraprotein dephosphorylation is that some sites may be more easily accessible compared with others and are therefore more readily dephosphorylated. We examined this by mapping the $\log_2$ ratios on to the 3D crystal structure of PKMYT1, a protein involved in regulating the auto-amplification loop of CDK1, which we identified as containing a high level of heterogeneously dephosphorylated sites (supplemental Fig. S6*A*). However, there was no obvious correlation with the level of dephosphorylation and the 3D location of the phosphosite, indicating that accessibility does not necessarily correlate with the dephosphorylation of specific sites within a protein.

Another possibility for this heterogeneity is that certain local amino acid sequences at and around the phosphorylation sites may be favored by phosphatases and are therefore preferentially dephosphorylated. To test this we performed comparative motif analysis between dephosphorylated and stable motifs for both S/T-P and Non-P sequences. Several distinct enrichments were correlated with dephosphorylation or with stable phosphosites (Fig. 7*A*). For Non-P sites, the presence of acidic amino acids (D/E) upstream (right), and to a lesser extent downstream (left) of the phosphorylation site strongly correlated with stable phosphosites, suggesting that these were impeding dephosphorylation (supplemental Fig. S6*B*). However, it should be noted that PLK1 and CK2 both favor acidic residues surrounding the phosphorylation site (supplemental Fig. S2), so this could simply reflect the continued activity of these kinases. In contrast, basic amino acids upstream (especially at +3 position) were highly enriched in dephosphorylated motifs, suggesting that these residues may promote dephosphorylation (supplemental Fig. S6*B*). For S/T-P sites, T sites were strongly and significantly dephosphorylated compared with total S/T-P site, whereas S sites were significantly more stable (Fig. 7*A*). This prominent preference for T over S was dependent on a P in the +1 position, as the preference for T was weakly, but not significantly seen in Non-P sites (supplemental Fig. S6*B*). Western blot analysis of synchronized mitotic exit samples using antibodies that specifically recognize SP or TP phosphorylated sites confirmed this observation, with global TP sites rapidly lost within 5 min of RO addition, whereas SP sites were slowly removed over the 120 min time-course (Fig. 7*B*).

Dephosphorylation of TP Sites is Regulated by Local Amino Acids—The above results suggest that TP sites are preferentially dephosphorylated compared with SP sites. However, only ~26% of all TP phosphosites were significantly dephos-

FIG. 5. **Dephosphorylation occurs on specific protein clusters during EME.** *A*, Comparison of the predicted upstream kinase for significantly dephosphorylated phosphosites, normalized against the total number of phosphosites identified for each kinase in the total data set. *B*, Proteins that contained a dephosphorylated Non-P and S/T-P site were compared and the common 156 proteins were subsequently subjected to STRING analysis to identify known and predicted protein-protein interactions. The 3 major clusters based on Gene Ontology (GO) are shown (yellow, green, blue). (*B* and *C*) Gene Ontology (GO) enrichment for Biological function (*B*) and Cellular Component (*C*) analysis was performed on proteins which contained commonly dephosphorylated or stable (no change) phosphorylation sites. The top 5 terms for dephosphorylated and no change were selected and compared. A false discovery rate (FDR) *p* value of <0.01 was considered significant. * Identifies terms that are significantly enriched only dephosphorylated or stable groups.

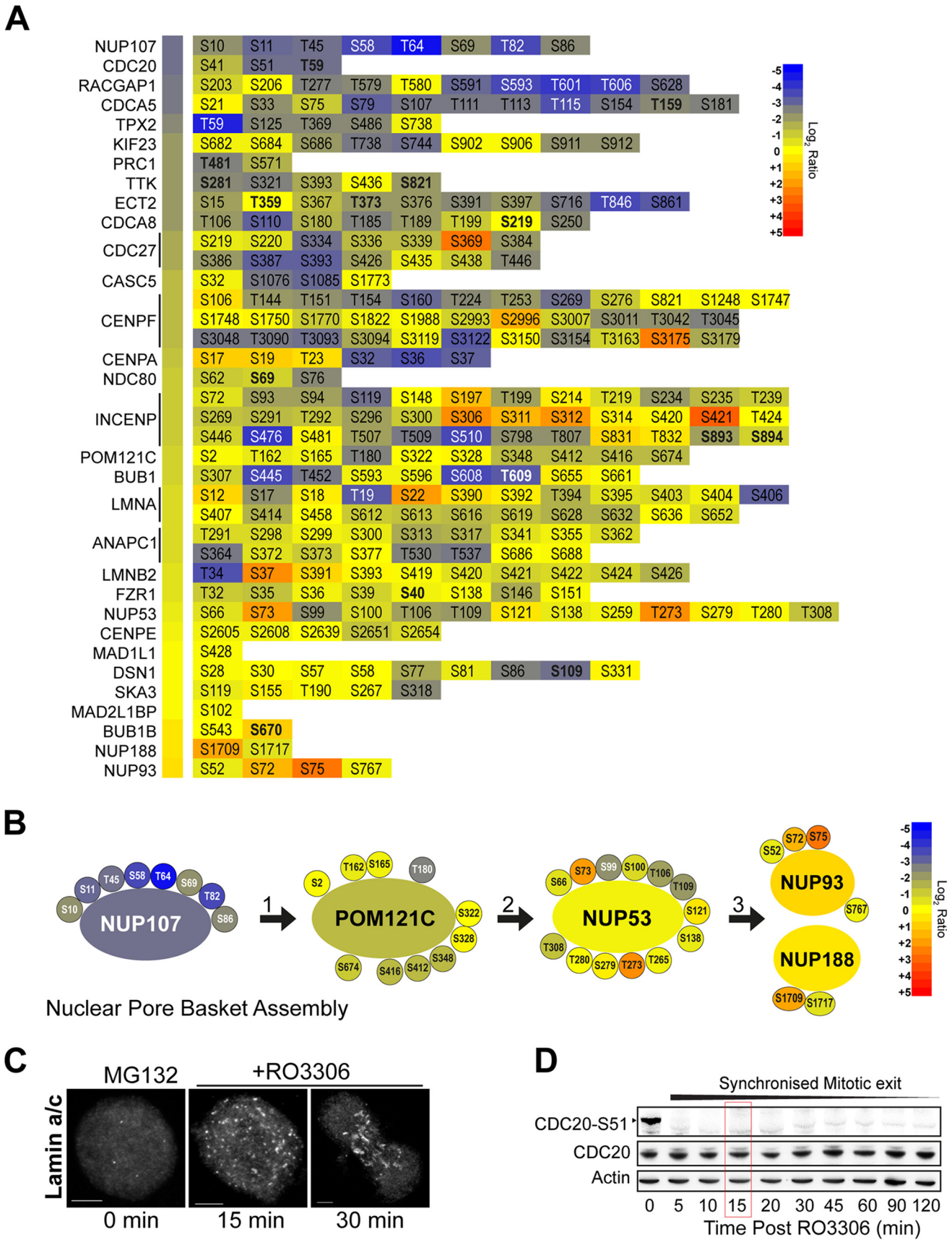
A
NUP107 S10 S11 T45 S58 T64 S69 T82 S86
CDC20 S41 S51 T59
RACGAP1 S203 S206 T277 T579 T580 S591 S593 T601 T606 S628
CDCA5 S21 S33 S75 S79 S107 T111 T113 T115 S154 T159 S181
TPX2 T59 S125 T369 S486 S738
KIF23 S682 S684 S686 T738 S744 S902 S906 S911 S912
PRC1 T481 S571
TTK S281 S321 S393 S436 S821
ECT2 S15 T359 S367 T373 S376 S391 S397 S716 T846 S861
CDCA8 T106 S110 S180 T185 T189 T199 S219 S250
CDC27 S219 S220 S334 S336 S339 S369 S384
S386 S387 S393 S426 S435 S438 T446
CASC5 S32 S1076 S1085 S1773
CENPF S106 T144 T151 T154 S160 T224 T253 S269 S276 S821 S1248 S1747
S1748 S1750 S1770 S1822 S1988 S2993 S2996 S3007 S3011 T3042 T3045
S3048 T3090 T3093 S3094 S3119 S3122 S3150 S3154 T3163 S3175 S3179
CENPA S17 S19 T23 S32 S36 S37
NDC80 S62 S69 S76
INCENP S72 S93 S94 S119 S148 S197 T199 S214 T219 S234 S235 T239
S269 S291 T292 S296 S300 S306 S311 S312 S314 S420 S421 T424
S446 S476 S481 T507 T509 S510 S798 T807 S831 T832 S893 S894
POM121C S2 T162 S165 T180 S322 S328 S348 S412 S416 S674
BUB1 S307 S445 T452 S593 S596 S608 T609 S655 S661
LMNA S12 S17 S18 T19 S22 S390 S392 T394 S395 S403 S404 S406
S407 S414 S458 S612 S613 S616 S619 S628 S632 S636 S652
ANAPC1 T291 S298 S299 S300 S313 S317 S341 S355 S362
S364 S372 S373 S377 T530 T537 S686 S688
LMNB2 T34 S37 S391 S393 S419 S420 S421 S422 S424 S426
FZR1 T32 S35 S36 S39 S40 S138 S146 S151
NUP53 S66 S73 S99 S100 T106 T109 S121 S138 S259 T273 S279 T280 T308
CENPE S2605 S2608 S2639 S2651 S2654
MAD1L1 S428
DSN1 S28 S30 S57 S58 S77 S81 S86 S109 S331
SKA3 S119 S155 T190 S267 S318
MAD2L1BP S102
BUB1B S543 S670
NUP188 S1709 S1717
NUP93 S52 S72 S75 S767
-5 -4 -3 -2 -1 0 +1 +2 +3 +4 +5
Log2 Ratio
B
NUP107
S10 S11 T45 S58 T64 S69 T82 S86
1
POM121C
S2 T162 S165 T180 S322 S328 S348 S412 S416 S674
2
NUP53
S66 S73 S99 S100 T106 T109 S121 S138 T265 T273 S279 T280 T308
3
NUP93
S52 S72 S75 S767
NUP188
S1709 S1717
-5 -4 -3 -2 -1 0 +1 +2 +3 +4 +5
Log2 Ratio
Nuclear Pore Basket Assembly
C
MG132
+RO3306
Lamin a/c
0 min
15 min
30 min
D
Synchronised Mitotic exit
CDC20-S51
CDC20
Actin
0 5 10 15 20 30 45 60 90 120
Time Post RO3306 (min)

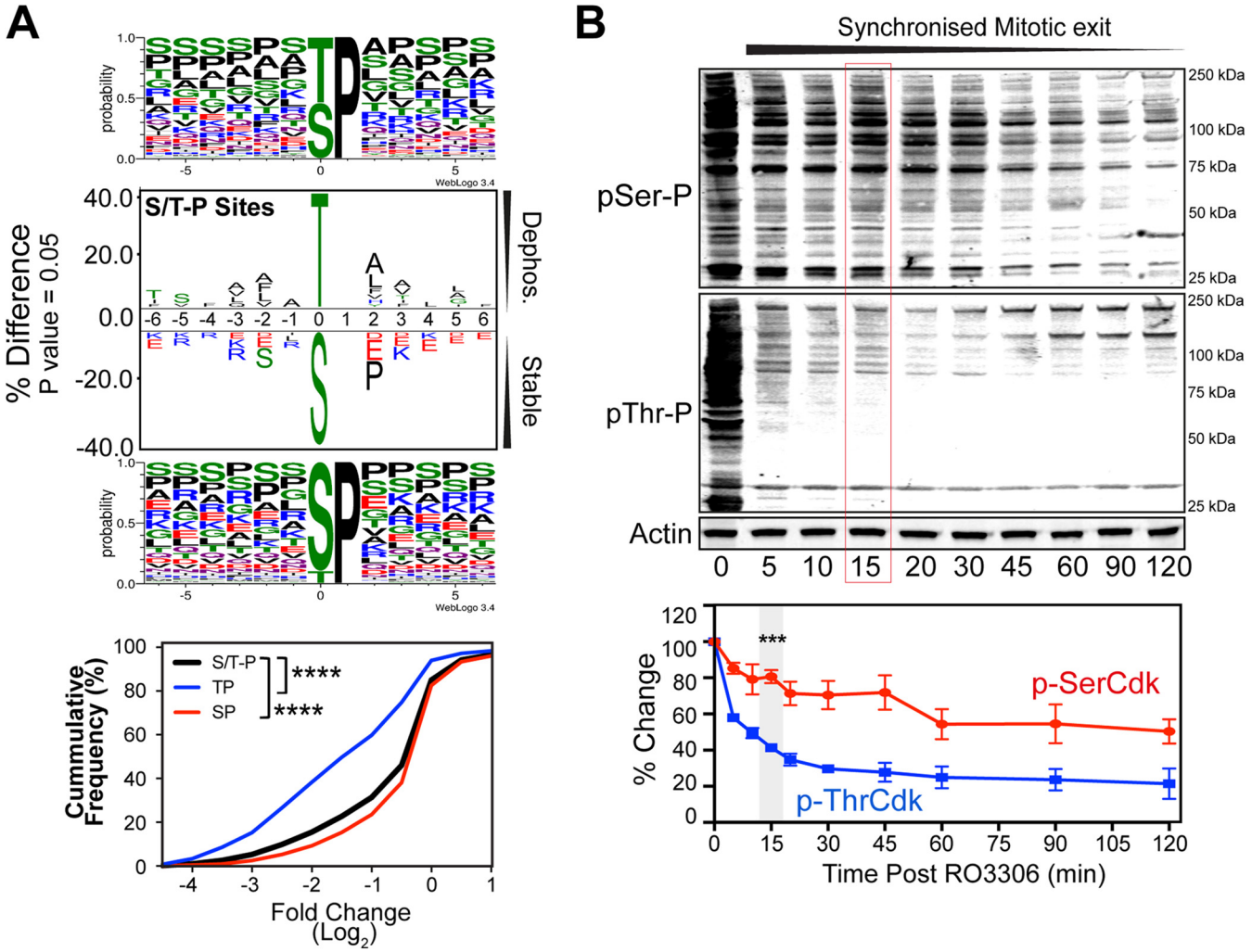

FIG. 7. **Local amino-acids predict phosphorylation status.** *A*, Dephosphorylated ($log_2 < -2$) and stable stable (log_2 −0. 25 to +0.25) S/T-P phosphopeptides were compared using IceLogo motif analysis software, to identify differentially enriched amino acids. Increasing letter size, and distance away from center, corresponds to stronger enrichment of amino acids. *B*, Validation of preferential dephosphorylation of TP compared with SP sites. HeLa cells were synchronized as per Fig. 1*A*, then harvested at the indicated times post-release, lysed, and analyzed by Western blot with antibodies that recognize proline directed phosphorylations at serine (pSer-P) and threonine (pThr-P) sites. Densitometry of 3 independent experiments was performed, normalized to actin and expressed as a percentage of 0 min time point. *p* value *** = <0.0001. All error bars are S.E.

phorylated during EME, indicating that additional factors beyond a TP were affecting dephosphorylation. Therefore, we analyzed TP sites in greater detail to determine if any additional amino acids surrounding the TP site correlated with dephosphorylation. Comparative motif alignments of dephosphorylated and stable TP sites showed that the +2 position played the strongest role in determining phosphorylation status (Fig. 8*A*). Specifically, small nonpolar amino acids (G, A, L, or V) were significantly enriched in dephosphorylated peptides (TPG motif). In contrast, a Proline at +2 (TPP motif) was significantly enriched in stable phosphopeptides, indicating that this residue inhibited dephosphorylation (Fig. 8*A* and 8*B*). Notably, similar enrichments were also found in SP sites (supplemental Fig. S6*C*). Comparing the TPG motif (dephos-

FIG. 6. **Intra-protein variations in neighboring phosphorylation sites.** *A*, Intraprotein phosphorylation changes of common proteins involved in regulation of EME. Proteins were ranked by the average fold change across all sites. Bold text indicates phosphorylation sites with a known role in regulating the function of the protein. *B*, Proteins from A involved in nuclear envelope reformation were ordered according to their mean log_2 ratio, which corresponded to the order of recruitment during nuclear envelope reassembly. *C*, HeLa cells were synchronized as per 1A treated with MG132 and then 15 min later RO3306, fixed at the indicated time-points, and stained with lamin a/c antibody. Partial reassembly of the nuclear envelope was observed at 15 min. All scale bars = 5 μm. (D) HeLa cells were synchronized as per Fig. 1A, then harvested at the indicated times post-release, lysed, and analyzed by Western blot with the indicated antibodies. Shown are representative blots from three independent experiments.

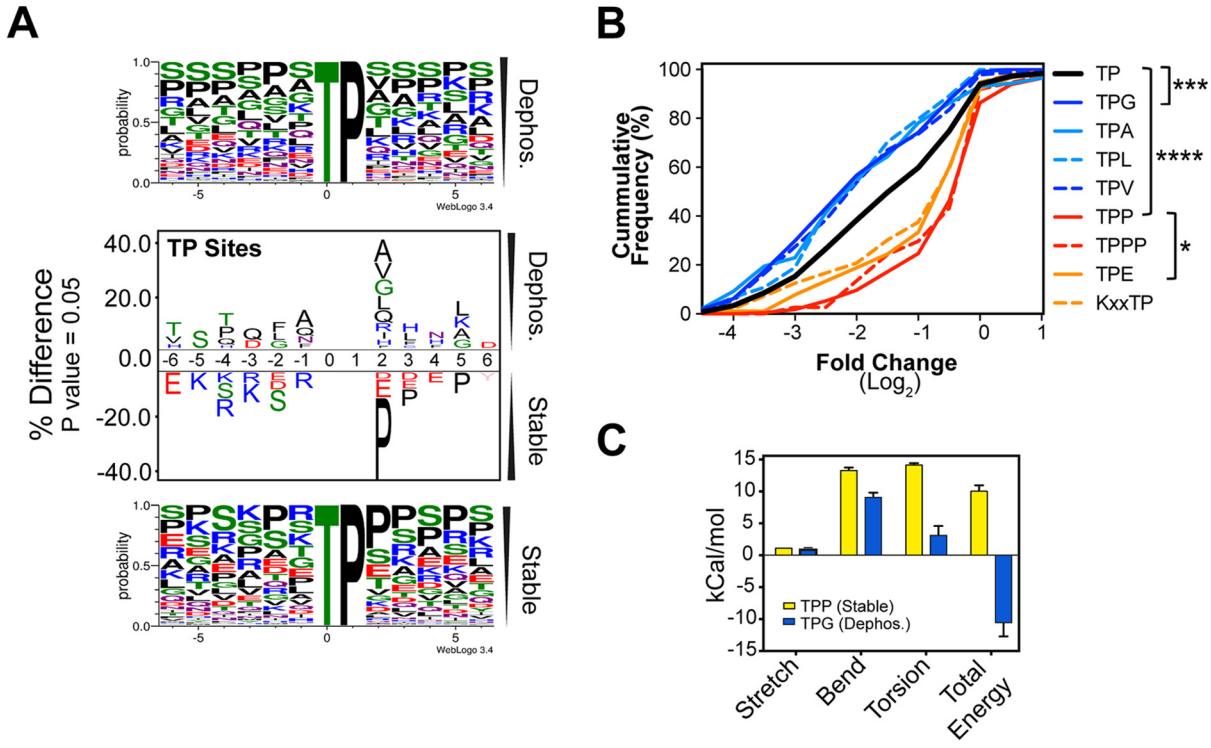

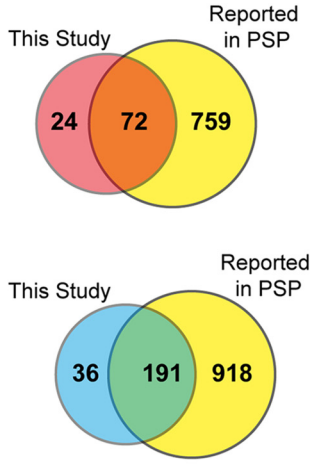

Gene	Site	Log2	Kinase	Phosphosite Function
CDC25B	T355	nd	p90RSK	Activation during G2/M
EIF4EBP1	T70	-0.2640	mTOR, Cdk1	Inhibits activity
FOXM1	T627	0.0688	Cdk4	Protein stabilization
JUNB	T255	0.2355	GSK3B	FBXW7 mediated degredation
MCL1	T163	nd	ERK1/2, JNK	Protein stabilization, Pin1 association
MED1	T1032	nd	ERK1/2	Activity induced, protein stabilization
MYC	T58	0.0058	GSK3	Pin1 and degradation
PKMYT1	T412	nd	?	Induces binding with Pin1
WDR77	T5	0.1605	Cdk4	Carcinogenesis
WEE1	T173	0.2711	?	? Degradation
ANLN	T364	-3.4772	?	?
CDC20	T59	-2.7717	?	?
CDC5L	T438	-3.2910	? Cdk	RNA splicing, altered
CDC7	T376	nd	Cdk1	enzymatic activity, induced
CDCA5	T159	-2.2600	Cdk1	Phosphorylation induces interaction with Plk1
CDCA8	T185	-2.4589	?	?
MASTL	T207	-2.4129	Cdk1?	Activation of Kinase
MEK1	T292	nd	Cdk1, Erk1/2	Inhibits activity
NUP133	T10	-2.0605	?	? Phosphorylated in mitosis
PRC1	T481	-2.1865	Cdk1	Prevents mid-zone localisation?

TPP Motif

TPG Motif

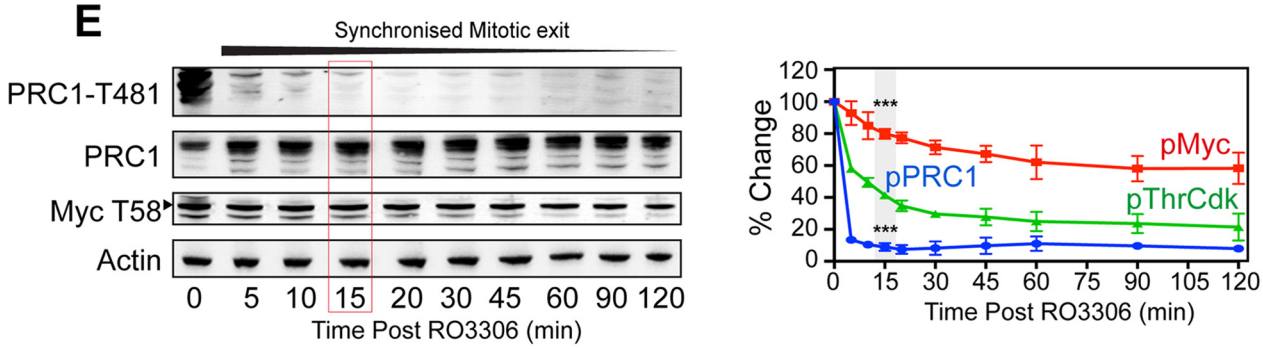

phorylated) to the stable TPP motif using MM2 molecular dynamics simulation and energy minimization illustrated that TPP has far greater energy associated with torsional strain (Fig. 8*C*). This indicates that the TPP is far more conformationally restricted than the TPG motif. The lower energy barrier to rotation could allow the TPG motif to switch to a geometry that is more favorable for dephosphorylation by a phosphatase.

Interestingly, phosphorylation on TPG and TPP motifs are currently annotated on 831 and 1109 proteins in PhosphoSitePlus respectively, and our analysis identified an additional 24 (TPG) and 36 (TPP) sites that have not previously been reported (Fig. 8*D*). These two motifs are evolutionarily conserved in numerous proteins such as FOXM1, JUNB, MYC, CDCA5 (Sororin) and PRC1, where they have known critical roles in regulating protein function (Fig. 8*D*, supplemental Figs. S7*A* and S7*B*). To validate these results we analyzed PRC1, a key regulator of cytokinesis and mid-spindle formation, and the transcription factor and oncogene MYC, as examples of a TPG and TPP motifs respectively. Phosphorylation at T481 prevents PRC1 from localizing to the central-spindle; therefore, rapid dephosphorylation at this site would be beneficial to ensure timely relocation of PRC1 during EME. Western blot analysis confirmed that this site is rapidly dephosphorylated during mitotic exit (Fig. 8*E*), which results in PRC1 relocating to the mid-spindle (supplemental Fig. S7*C*). In contrast, phosphorylation of the TPP motif in MYC was highly stable during mitotic exit with significant levels of phosphorylation on T58 still present 120 min after triggering of mitotic exit (Fig. 8*E*). Interestingly, the residues from T58 to S60 are a hot spot for missense mutation in cancer (supplemental Fig. S7*D*), with the annotated mutation of P60A observed in cancer cell lines creating at TPA motif, which our modeling predicts to be rapidly dephosphorylated (Fig. 8*A*). In summary, these results suggest that phosphorylation on the physically restrictive TPP motif is highly stable, whereas the more flexible TPG motif is more readily dephosphorylated.

DISCUSSION

This study shows that during EME in human cells, only a small fraction of protein phosphorylation modifications are removed and responsible for the events that occur during anaphase. Not surprisingly, these dephosphorylation events occur on proteins that are involved in regulating nuclear pore assembly, central-spindle formation, and SAC function, which are all critical for these EME events. Consequently, dephosphorylation is critical for ensuring that mitotic exit occurs in the correct order. This raises an important question of how specific dephosphorylation of these critical EME proteins is determined. One possibility is that as cells exit mitosis, kinase activity decreases, shifting the balance toward dephosphorylation. Many kinases have well established preferences for certain substrates, and this preference could determine the rate as which specific sites and proteins are dephosphorylated. However, our results suggest that there are additional factors beyond kinase activity that determine specificity. First, our use of a specific CDK1 inhibitor did not result in a preferential dephosphorylation of CDK1 substrates, suggesting that the activity of CDK1 does not necessarily determine the specific dephosphorylation of EME substrates. This is supported by work in yeast, which showed during early mitotic exit, the specificity of CDK toward specific substrates did not correlate with substrate dephosphorylation. Furthermore, forced persistent CDK activity during exit only prevented the dephosphorylation of late mitotic exit substrates, with EME substrates continuing to be dephosphorylated independently of CDK activity (8). We also found that there was a similar enrichment of EME proteins dephosphorylated across all the kinases we analyzed, reducing the likelihood that kinase activity and/or specificity is driving the order of dephosphorylation during EME.

Therefore, specific dephosphorylation of EME proteins must be driven by the activity of phosphatases. In support, inhibition of phosphatases with okadaic acid prevented mitotic exit and dephosphorylation, indicating that the PP1/2A/4/6 families of phosphatases are responsible for dephosphorylating substrates during EME. This is supported by previous studies which have shown that both PP1 (23, 59, 60) and PP2A (45, 57, 61) are responsible for dephosphorylating critical substrates during EME in mammals. However, this still does not answer the question of how these phosphatases specifically dephosphorylate only a discrete subset of phosphorylation sites during EME. The answer in part is likely because of the nature of these families of phosphatases, which are multimeric protein complexes that can be regulated by a variety of mechanisms. These include the binding of

FIG. 8. **Evolutionary conserved TPP and TPG motifs dictate phosphorylation status.** *A*, Similar to 7B, dephosphorylated (dephos.) and stable (stable) sites from TP phosphorylated phosphopeptides were compared using IceLogo software. *B*, The distribution of all phosphopeptides corresponding to the top dephosphorylated and stable motifs were compared, with significant differences (*p* values) shown. *p* values * = <0.01, ** = <0.001, *** = <0.0001, **** = <0.00001, NS = not significant. *C*, Comparison of stretch, bend, torsion and total energy requirements of the TPP and TPG short peptide motifs using MM2 dynamics simulation. *D*, Venn diagrams comparing the number of proteins identified with a phosphorylated TPP or TPG motif in our MS data compared with PhosphoSitePlus. A table of 10 notable proteins from PhosphoSitePlus and our data set that contain the TPP and TPG motifs, the upstream phosphorylating kinase, and the function this phosphorylation has on protein function. *E*, Dephosphorylation of PRC1-T481 TPG motif and stability of MYC-T58 TPP motif. Briefly, HeLa cells were synchronized as per Fig. 1*A*, then harvested at the indicated times post-release, lysed, and analyzed by Western blot with the indicated antibodies. Densitometry of three independent experiments was performed, normalized to actin and expressed as a percentage of 0 min time point. *t* tests were performed to compare pPRC1 (blue) or pMYC (red) to total pThr-P sites (green). *p* value *** = <0.0001. All error bars are S.E.

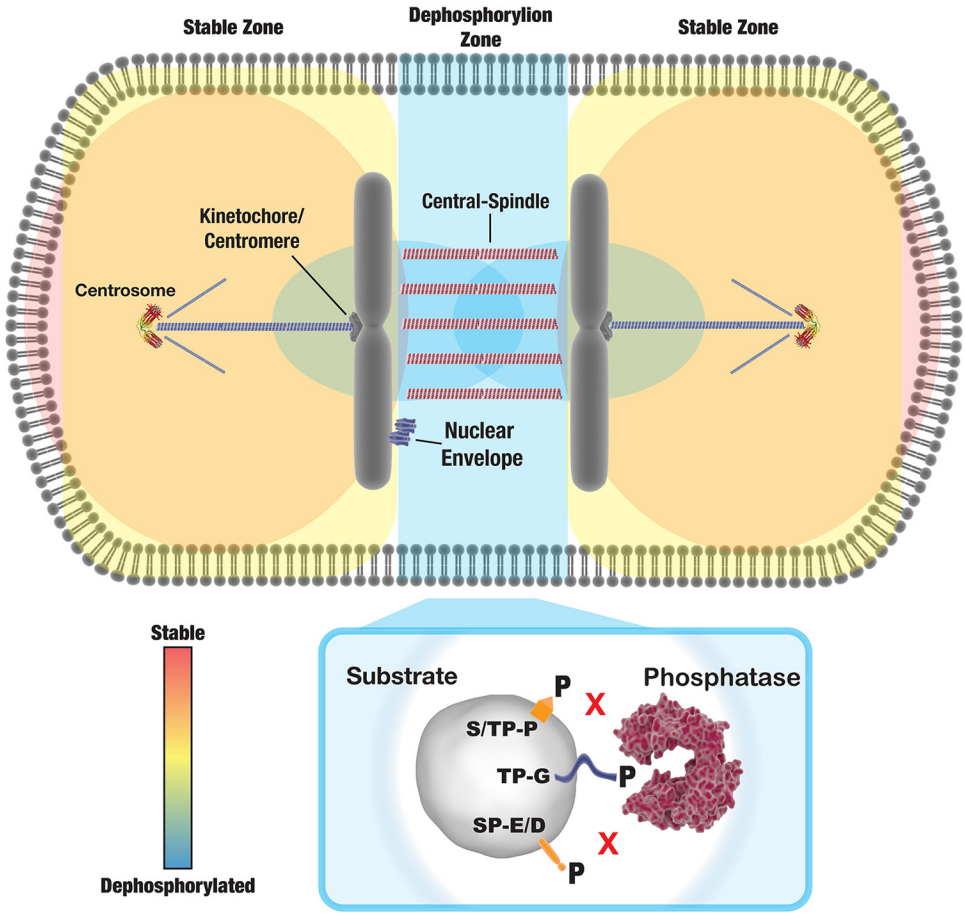

FIG. 9. **Proposed model of mechanisms controlling specific dephosphorylation during EME.** Proteins that are involved in regulating midspindle formation, kinetochore function and nuclear pore assembly are preferentially dephosphorylated (blue) during EME. In addition, specific amino acids at and surrounding the phosphorylation site on individual proteins, helps dictate the dephosphorylation. Together these two mechanisms help provide the specific dephosphorylation pattern and ordering of events during mitotic exit.

regulatory subunits and inhibitory proteins, which can target these phosphatases to specific subcellular localizations (reviewed in (62, 63)). For example, during mitosis PP2A bound with the B56 regulatory subunit (PP2A-B56) is targeted to the kinetochore region (57) and PP2A-B55 to the mitotic spindle (64), where they plays critical roles in silencing the SAC and activating the APC respectively. Likewise, PP1-RepoMan (cdca2) is also targeted to the kinetochore region, where it regulates the microtubule-kinetochore interface during anaphase (65). PP1 in combination with Sds22 is targeted to the cell cortex (66), chromatin via PNUTs (59), and binding with AKAP149 targets to the nuclear envelope (67). Targeting of PP1 and PP2A to these regions corresponds with the proteins that we found to be dephosphorylated during EME, and therefore sub-cellular localization clearly plays a key role in determining the specificity of the phosphatases (Fig. 9). However, it does not explain why some proteins at these locations are not dephosphorylated, or the large variation in dephosphorylation of neighboring sites seen in many individual proteins observed at these subcellular locations.

Our results suggest that local amino acids at and around the phosphorylation site could provide a mechanism for the specificity of the phosphatases. This was most clearly observed with Proline directed sites, which showed a strong preference for dephosphorylation of Threonine compared with Serine residues. Malik *et al.* also observed a similar preference for the dephosphorylation of TP sites during mitotic exit (50), whereas *in vitro* dephosphorylation assays using synthetic peptides also found TP sites were heavily favored over SP sites (68). Our results also identified that residues surrounding the phosphorylation site have an impact on dephosphorylation. For Non-P directed motifs, acidic amino acids with negatively charged side chains (D, E) upstream from the phosphorylation site appear to protect and prevent dephosphorylation, whereas basic amino acids (K, R) generally promote dephosphorylation (supplementary Fig. S6*B*). In support, arginine (R) residues proximal to the (S31/S40) phosphorylation sites in tyrosine hydroxylase have been shown to promote dephosphorylation by PP2A (69). For Proline directed motifs, the amino acid at the +2 position heavily

impacts dephosphorylation. Specifically, small non-polar residues (*e.g.* G, A,V, and L) promote dephosphorylation. This was best exemplified by the evolutionary conserved TPG motif found in PRC1, which is rapidly dephosphorylated during EME prompting its relocation to the central-spindle. We also identified several inhibitory motifs that prevented dephosphorylation, with a Proline or glutamic acid at the +2 position (S/T-P-P/E motif) strongly correlating with stable phosphorylation sites. Interestingly, there are several well-known TPP motifs in proteins such as MYC, JunB, and FoxM1, which have all been found to play critical roles in regulating the degradation and function of these proteins. For example, phosphorylation of the TPP site in MYC (T58) is required for efficient degradation of MYC. Phosphorylation at T58 and the upstream S62, provides a docking site for the isomerase Pin1, which then promotes the *cis-trans* conformational change between the S62-P63 bond. This allows PP2A to bind and dephosphorylate the S63 site, which in turn creates a motif for targeting MYC for degradation (70). This could also be an explanation for why the T58-P60 site is commonly mutated in a range of cancers (71, 72), as rapid dephosphorylation of the T58 site would prevent MYC from being degraded, thereby promoting MYC accumulation, and increased MYC-dependent transcription. This regulation of protein degradation by the stable and rigid TPP motif could be a more general mechanism, as many of the proteins we identified with at TPP motif (*e.g.* Mcl-1, JunB, FoxM1, Myt1) are associated with Pin1 and regulation of protein degradation.

In summary, our results provide a global overview of the tens of thousands of phosphorylation sites regulated by multiple kinases during mitosis, providing an invaluable resource for the wider research community. Furthermore, we have shown that EME is driven by specific dephosphorylation by phosphatases of only a small subset of these phosphorylation sites. Finally, we have identified that the precise dephosphorylation of specific residues is driven in part by unique amino acid residues at and surrounding the phosphorylation site, providing a mechanistic explanation for how phosphatases drive the ordered dephosphorylation of substrates and drive the coordinated events of mitotic exit.

Acknowledgments—We thank Sylvain De Rossi (Montpellier RIO Imaging), P Richard (Animal Facility), Gillian Lehrbach (Tissue Culture), Sean J. Humphrey, Daniel J. Fazakerley and Mark Cowley for assistance. We thank Darren Saunders and David Gallego Ortega for their helpful comments and the PRIDE Team at the ProteomeXchange Consortium. Grateful acknowledgments are due to N Morin, TU Mayer for anti-TPX2 and anti-Mklp2 antibodies. A.B. is a CINSW FRL fellow.

This article contains supplemental Tables S1 and S2, Figs. S1 to S7 and Video S1.

§§ To whom correspondence should be addressed: Garvan Institute of Medical Research, Darlinghurst 370 Victoria St, Sydney, NS 2010 Australia. Tel.: Australia-02–9355 5777; E-mail: a.burgess@garvan.org.au.

REFERENCES

1. Johnson, L. N. (2011) Substrates of mitotic kinases. *Sci. Signal.* **4,** pe31–pe31
2. Nigg, E. A. (2001) Mitotic kinases as regulators of cell division and its checkpoints. *Nat. Rev. Mol. Cell Biol.* **2,** 21–32
3. Dephoure, N., Zhou, C., Villén, J., Beausoleil, S. A., Bakalarski, C. E., Elledge, S. J., and Gygi, S. P. (2008) A quantitative atlas of mitotic phosphorylation. *Proc. Natl. Acad. Sci. U.S.A.* **105,** 10762–10767
4. Daub, H., Olsen, J. V., Bairlein, M., Gnad, F., Oppermann, F. S., Körner, R., Greff, Z., Kéri, G., Stemmann, O., and Mann, M. (2008) Kinase-selective enrichment enables quantitative phosphoproteomics of the kinome across the cell cycle. *Mol. Cell* **31,** 438–448
5. Kettenbach, A. N., Schweppe, D. K., Faherty, B. K., Pechenick, D., Pletnev, A. A., and Gerber, S. A. (2011) Quantitative phosphoproteomics identifies substrates and functional modules of Aurora and Polo-like kinase activities in mitotic cells. *Sci. Signal*. **4,** rs5–rs5
6. Wurzenberger, C., and Gerlich, D. W. (2011) Phosphatases: providing safe passage through mitotic exit. *Nat. Rev. Mol. Cell Biol.* **12,** 469–482
7. Sullivan, M., and Morgan, D. O. (2007) Finishing mitosis, one step at a time. *Nat. Rev. Mol. Cell Biol.* **8,** 894–903
8. Bouchoux, C., and Uhlmann, F. (2011) A quantitative model for ordered Cdk substrate dephosphorylation during mitotic exit. *Cell* **147,** 803–814
9. Izawa, D., and Pines, J. (2011) How APC/C-Cdc20 changes its substrate specificity in mitosis. *Nat. Cell Biol.* **13,** 223–233
10. Matsusaka, T., Enquist-Newman, M., Morgan, D. O., and Pines, J. (2014) Co-activator independent differences in how the metaphase and anaphase APC/C recognise the same substrate. *Biol. Open* **3,** 904–912
11. Potapova, T. A., Daum, J. R., Pittman, B. D., Hudson, J. R., Jones, T. N., Satinover, D. L., Stukenberg, P. T., and Gorbsky, G. J. (2006) The reversibility of mitotic exit in vertebrate cells. *Nature* **440,** 954–958
12. López-Avilés, S., Kapuy, O., Novák, B., and Uhlmann, F. (2009) Irreversibility of mitotic exit is the consequence of systems-level feedback. *Nature* **459,** 592–595
13. Min, M., Mayor, U., Dittmar, G., and Lindon, C. (2014) Using in vivo biotinylated ubiquitin to describe a mitotic exit ubiquitome from human cells. *Mol. Cell Proteomics* **13,** 2411–2425
14. Olsen, J. V., Vermeulen, M., Santamaria, A., Kumar, C., Miller, M. L., Jensen, L. J., Gnad, F., Cox, J., Jensen, T. S., Nigg, E. A., Brunak, S., and Mann, M. (2010) Quantitative phosphoproteomics reveals widespread full phosphorylation site occupancy during mitosis. *Sci. Signal.* **3,** ra3–ra3
15. Mochida, S., Ikeo, S., Gannon, J., and Hunt, T. (2009) Regulated activity of PP2A–B55δ is crucial for controlling entry into and exit from mitosis in Xenopus egg extracts. *EMBO J.* **28,** 2777–2785
16. Vigneron, S., Brioudes, E., Burgess, A., Labbé, J. C., Lorca, T., and Castro, A. (2009) Greatwall maintains mitosis through regulation of PP2A. *EMBO J.* **28,** 2786–2793
17. Burgess, A., Vigneron, S., Brioudes, E., Labbé, J. C., Lorca, T., and Castro, A. (2010) Loss of human Greatwall results in G2 arrest and multiple mitotic defects due to deregulation of the cyclin B-Cdc2/PP2A balance. *Proc. Natl. Acad. Sci. U.S.A.* **107,** 12564–12569
18. McCloy, R. A., Rogers, S., Caldon, C. E., Lorca, T., Castro, A., and Burgess, A. (2014) Partial inhibition of Cdk1 in G2 phase overrides the SAC and decouples mitotic events. *Cell Cycle* **13,** 1400–1412
19. De Wulf, P., Montani, F., and Visintin, R. (2009) Protein phosphatases take the mitotic stage. *Curr. Opin. Cell Biol.* **21,** 806–815
20. Schmitz, M. H., Held, M., Janssens, V., Hutchins, J. R., Hudecz, O., Ivanova, E., Goris, J., Trinkle-Mulcahy, L., Lamond, A. I., Poser, I., Hyman, A. A., Mechtler, K., Peters, J. M., and Gerlich, D. W. (2010) Live-cell imaging RNAi screen identifies PP2A-B55alpha and importin-beta1 as key mitotic exit regulators in human cells. *Nat. Cell Biol.* **12,** 886–893
21. Mayer-Jaekel, R. E., Ohkura, H., Gomes, R., Sunkel, C. E., Baumgartner, S., Hemmings, B. A., and Glover, D. M. (1993) The 55 kd regulatory subunit of Drosophila protein phosphatase 2A is required for anaphase. *Cell* **72,** 621–633
22. Manchado, E., Guillamot, M., de Cárcer, G., Eguren, M., Trickey, M., García-Higuera, I., Moreno, S., Yamano, H., Cañamero, M., and Malumbres, M. (2010) Targeting mitotic exit leads to tumor regression in vivo: Modulation by Cdk1, Mastl, and the PP2A/B55α,δ phosphatase. *Cancer Cell* **18,** 641–654

23. Wu, J. Q., Guo, J. Y., Tang, W., Yang, C. S., Freel, C. D., Chen, C., Nairn, A. C., and Kornbluth, S. (2009) PP1-mediated dephosphorylation of phosphoproteins at mitotic exit is controlled by inhibitor-1 and PP1 phosphorylation. *Nat. Cell Biol.* **11,** 644–651
24. Meadows, J. C. (2013) Interplay between mitotic kinesins and the Aurora kinase-PP1 (protein phosphatase 1) axis. *Biochem. Soc. Trans.* **41,** 1761–1765
25. Mocciaro, A., and Schiebel, E. (2010) Cdc14: a highly conserved family of phosphatases with non-conserved functions? *J. Cell Sci.* **123,** 2867–2876
26. Larsen, M. R., Thingholm, T. E., Jensen, O. N., Roepstorff, P., and Jørgensen, T. J. D. (2005) Highly selective enrichment of phosphorylated peptides from peptide mixtures using titanium dioxide microcolumns. *Mol. Cell. Proteomics* **4,** 873–886
27. Olsen, J. V., Blagoev, B., Gnad, F., Macek, B., Kumar, C., Mortensen, P., and Mann, M. (2006) Global, in vivo, and site-specific phosphorylation dynamics in signaling networks. *Cell* **127,** 635–648
28. Cox, J., Neuhauser, N., Michalski, A., Scheltema, R. A., Olsen, J. V., and Mann, M. (2011) Andromeda: a peptide search engine integrated into the MaxQuant environment. *J. Proteome Res.* **10,** 1794–1805
29. Ritchie, M. E., Phipson, B., Wu, D., Hu, Y., Law, C. W., Shi, W., and Smyth, G. K. (2015) limma powers differential expression analyses for RNA-sequencing and microarray studies. *Nucleic Acids Res.* **43,** e47
30. Vizcaíno, J. A., Côté, R. G., Csordas, A., Dianes, J. A., Fabregat, A., Foster, J. M., Griss, J., Alpi, E., Birim, M., Contell, J., O'Kelly, G., Schoenegger, A., Ovelleiro, D., Pérez-Riverol, Y., Reisinger, F., Ríos, D., Wang, R., and Hermjakob, H. (2013) The PRoteomics IDEntifications (PRIDE) database and associated tools: Status in 2013. *Nucleic Acids Res.* **41,** D1063–D9
31. Baker, P. R., and Chalkley, R. J. (2014) MS-viewer: a web-based spectral viewer for proteomics results. *Mol. Cell. Proteomics* **13,** 1392–1396
32. Franceschini, A., Szklarczyk, D., Frankild, S., Kuhn, M., Simonovic, M., Roth, A., Lin, J., Minguez, P., Bork, P., Mering, von, C., and Jensen, L. J. (2013) STRING v9.1: protein-protein interaction networks, with increased coverage and integration. *Nucleic Acids Res.* **41,** D808–D15
33. Chen, E. Y., Tan, C. M., Kou, Y., Duan, Q., Wang, Z., Meirelles, G. V., Clark, N. R., and Ma'ayan, A. (2013) Enrichr: interactive and collaborative HTML5 gene list enrichment analysis tool. *BMC Bioinformatics* **14,** 128
34. Wang, T., Kettenbach, A. N., Gerber, S. A., and Bailey-Kellogg, C. (2012) MMFPh: a maximal motif finder for phosphoproteomics datasets. *Bioinformatics* **28,** 1562–1570
35. Colaert, N., Helsens, K., Martens, L., Vandekerckhove, J., and Gevaert, K. (2009) Improved visualization of protein consensus sequences by iceLogo. *Nat. Methods* **6,** 786–787
36. Crooks, G. E., Hon, G., Chandonia, J. M., and Brenner, S. E. (2004) WebLogo: a sequence logo generator. *Genome Res.* **14,** 1188–1190
37. Horn, H., Schoof, E. M., Kim, J., Robin, X., Miller, M. L., Diella, F., Palma, A., Cesareni, G., Jensen, L. J., and Linding, R. (2014) KinomeXplorer: an integrated platform for kinome biology studies. *Nat. Methods* **11,** 603–604
38. Pavlidis, P., and Noble, W. S. (2003) Matrix2png: a utility for visualizing matrix data. *Bioinformatics* **19,** 295–296
39. Kearse, M., Moir, R., Wilson, A., Stones-Havas, S., Cheung, M., Sturrock, S., Buxton, S., Cooper, A., Markowitz, S., Duran, C., Thierer, T., Ashton, B., Meintjes, P., and Drummond, A. (2012) Geneious Basic: an integrated and extendable desktop software platform for the organization and analysis of sequence data. *Bioinformatics* **28,** 1647–1649
40. Lii, J. H., Gallion, S., Bender, C., Wikstr m, H. K., Allinger, N. L., Flurchick, K. M., and Teeter, M. M. (1989) Molecular mechanics (MM2) calculations on peptides and on the protein Crambin using the CYBER 205. *J. Comput. Chem.* **10,** 503–513
41. Steigemann, P., Wurzenberger, C., Schmitz, M. H.., Held, M., Guizetti, J., Maar, S., and Gerlich, D. W. (2009) Aurora B-mediated abscission checkpoint protects against tetraploidization. *Cell* **136,** 473–484
42. Wolf, F., Sigl, R., and Geley, S. (2007) ". The end of the beginning": cdk1 thresholds and exit from mitosis. *Cell Cycle* **6,** 1408–1411
43. Vassilev, L. T., Tovar, C., Chen, S., Knezevic, D., Zhao, X., Sun, H., Heimbrook, D. C., and Chen, L. (2006) Selective small-molecule inhibitor reveals critical mitotic functions of human CDK1. *Proc. Natl. Acad. Sci. U.S.A.* **103,** 10660–10665
44. Potapova, T. A., Sivakumar, S., Flynn, J. N., Li, R., and Gorbsky, G. J. (2011) Mitotic progression becomes irreversible in prometaphase and collapses when Wee1 and Cdc25 are inhibited. *Mol. Biol. Cell* **22,** 1191–1206
45. Cundell, M. J., Bastos, R. N., Zhang, T., Holder, J., Gruneberg, U., Novák, B., and Barr, F. A. (2013) The BEG (PP2A-B55/ENSA/Greatwall) pathway ensures cytokinesis follows chromosome separation. *Mol. Cell* **52,** 393–405
46. Vázquez-Novelle, M. D., Sansregret, L., Dick, A. E., Smith, C. A., McAinsh, A. D., Gerlich, D. W., and Petronczki, M. (2014) Cdk1 inactivation terminates mitotic checkpoint surveillance and stabilizes kinetochore attachments in anaphase. *Current Biol.* **24,** 638–645
47. Hagting, A., Elzen, Den, N., Vodermaier, H. C., Waizenegger, I. C., Peters, J. M., and Pines, J. (2002) Human securin proteolysis is controlled by the spindle checkpoint and reveals when the APC/C switches from activation by Cdc20 to Cdh1. *J. Cell Biol.* **157,** 1125–1137
48. Hornbeck, P. V., Kornhauser, J. M., Tkachev, S., Zhang, B., Skrzypek, E., Murray, B., Latham, V., and Sullivan, M. (2012) PhosphoSitePlus: a comprehensive resource for investigating the structure and function of experimentally determined post-translational modifications in man and mouse. *Nucleic Acids Res.* **40,** D261–D70
49. Ozlü, N., Monigatti, F., Renard, B. Y., Field, C. M., Steen, H., Mitchison, T. J., and Steen, J. J. (2010) Binding partner switching on microtubules and aurora-B in the mitosis to cytokinesis transition. *Mol. Cell Proteomics* **9,** 336–350
50. Malik, R., Lenobel, R., Santamaria, A., Ries, A., Nigg, E. A., and Körner, R. (2009) Quantitative Analysis of the Human Spindle Phosphoproteome at Distinct Mitotic Stages. *J. Proteome Res.* **8,** 4553–4563
51. Amanchy, R., Periaswamy, B., Mathivanan, S., Reddy, R., Tattikota, S. G., and Pandey, A. (2007) A curated compendium of phosphorylation motifs. *Nat. Biotechnol.* **25,** 285–286
52. Suzuki, K., Sako, K., Akiyama, K., Isoda, M., Senoo, C., Nakajo, N., and Sagata, N. (2015) Identification of non-Ser/Thr-Pro consensus motifs for Cdk1 and their roles in mitotic regulation of C2H2 zinc finger proteins and Ect2. *Sci. Rep.* **5,** 7929
53. Santamaria, A., Neef, R., Eberspächer, U., Eis, K., Husemann, M., Mumberg, D., Prechtl, S., Schulze, V., Siemeister, G., Wortmann, L., Barr, F. A., and Nigg, E. A. (2007) Use of the novel Plk1 inhibitor ZK-thiazolidinone to elucidate functions of Plk1 in early and late stages of mitosis. *Mol. Biol. Cell* **18,** 4024–4036
54. Schooley, A., Vollmer, B., and Antonin, W. (2012) Building a nuclear envelope at the end of mitosis: coordinating membrane reorganization, nuclear pore complex assembly, and chromatin de-condensation. *Chromosoma* **121,** 539–554
55. Huang, H., Hittle, J., Zappacosta, F., Annan, R. S., Hershko, A., and Yen, T. J. (2008) Phosphorylation sites in BubR1 that regulate kinetochore attachment, tension, and mitotic exit. *J. Cell Biol.* **183,** 667–680
56. Kruse, T., Zhang, G., Larsen, M. S., Lischetti, T., Streicher, W., Kragh Nielsen, T., Bjørn, S. P., and Nilsson, J. (2013) Direct binding between BubR1 and B56-PP2A phosphatase complexes regulate mitotic progression. *J. Cell Sci.* **126,** 1086–1092
57. Espert, A., Uluocak, P., Bastos, R. N., Mangat, D., Graab, P., and Gruneberg, U. (2014) PP2A-B56 opposes Mps1 phosphorylation of Knl1 and thereby promotes spindle assembly checkpoint silencing. *J. Cell Biol.* **206,** 833–842
58. Cui, Y., Cheng, X., Zhang, C., Zhang, Y., Li, S., Wang, C., and Guadagno, T. M. (2010) Degradation of the human mitotic checkpoint kinase Mps1 is cell cycle-regulated by APC-cCdc20 and APC-cCdh1 ubiquitin ligases. *J. Biol. Chem.* **285,** 32988–32998
59. Fisher, L. A., Wang, L., Wu, L., and Peng, A. (2014) Phosphatase 1 nuclear targeting subunit is an essential regulator of M-phase entry, maintenance, and exit. *J. Biol. Chem.* **289,** 23745–23752
60. London, N., Ceto, S., Ranish, J. A., and Biggins, S. (2012) Phosphoregulation of Spc105 by Mps1 and PP1 regulates Bub1 localization to kinetochores. *Curr. Biol.* **22,** 900–906
61. Hellmuth, S., Böttger, F., Pan, C., Mann, M., and Stemmann, O. (2014) PP2A delays APC/C-dependent degradation of separase-associated but not free securin. *EMBO J.* **33,** 1134–1147
62. Slupe, A. M., Merrill, R. A., and Strack, S. Determinants for Substrate Specificity of Protein Phosphatase 2A. *Enzyme Res.* 2011:398751–8, 2011
63. Bollen, M., Peti, W., Ragusa, M. J., and Beullens, M. (2010) The extended PP1 toolkit: designed to create specificity. *Trends Biochem. Sci.* **35,** 450–458

64. Torres, J. Z., Ban, K. H., and Jackson, P. K. (2010) A specific form of phospho protein phosphatase 2 regulates anaphase-promoting complex/cyclosome association with spindle poles. *Mol. Biol. Cell* **21,** 897–904
65. Wurzenberger, C., Held, M., Lampson, M. A., Poser, I., Hyman, A. A., and Gerlich, D. W. (2012) Sds22 and Repo-Man stabilize chromosome segregation by counteracting Aurora B on anaphase kinetochores. *J. Cell Biol.* **198,** 173–183
66. Kunda, P., Rodrigues, N. T., Moeendarbary, E., Liu, T., Ivetic, A., Charras, G., and Baum, B. (2012) PP1-mediated moesin dephosphorylation couples polar relaxation to mitotic exit. *Curr. Biol.* **22,** 231–236
67. Steen, R. L., Beullens, M., Landsverk, H. B., Bollen, M., and Collas, P. (2003) AKAP149 is a novel PP1 specifier required to maintain nuclear envelope integrity in G1 phase. *J. Cell Sci.* **116,** 2237–2246
68. Agostinis, P., Goris, J., Pinna, L. A., Marchiori, F., Perich, J. W., Meyer, H. E., and Merlevede, W. (1990) Synthetic peptides as model substrates for the study of the specificity of the polycation-stimulated protein phosphatases. *Eur. J. Biochem.* **189,** 235–241
69. Saraf, A., Oberg, E. A., and Strack, S. (2010) Molecular determinants for PP2A substrate specificity: charged residues mediate dephosphorylation of tyrosine hydroxylase by the PP2A/B' regulatory subunit. *Biochemistry* **49,** 986–995
70. Arnold, H. K., and Sears, R. C. (2006) Protein Phosphatase 2A Regulatory Subunit B56 Associates with c-Myc and Negatively Regulates c-Myc Accumulation. *Mol. Cell. Biol.* **26,** 2832–2844
71. Bhatia, K., Huppi, K., Spangler, G., Siwarski, D., Iyer, R., and Magrath, I. (1993) Point mutations in the c-Myc transactivation domain are common in Burkitt's lymphoma and mouse plasmacytomas. *Nat. Genet.* **5,** 56–61
72. Bahram, F., Lehr, von der, N., Cetinkaya, C., and Larsson, L. G. (2000) c-Myc hot spot mutations in lymphomas result in inefficient ubiquitination and decreased proteasome-mediated turnover. *Blood* **95,** 2104–2110